Controlling Aspects of the Switched Reluctance Motor for Automotive and Industrial Applications

Dissertation submitted to
Visvesvaraya National Institute of Technology, Nagpur
in partial fulfilment of requirements for the award of
degree of

Master of Technology
in
Integrated Power System

by

Sandeep Kumar Dehuri
(MT23IPS002)

under the Guidance of

Dr. M. M. Lokhande
Associate Professor

DEPARTMENT OF ELECTRICAL ENGINEERING
VISVESVARAYA NATIONAL INSTITUTE OF TECHNOLOGY (VNIT)
June 2025

Controlling Aspects of the Switched Reluctance Motor for Automotive and Industrial Applications

Dissertation submitted to
Visvesvaraya National Institute of Technology, Nagpur
in partial fulfilment of requirements for the award of
degree of

Master of Technology
in
Integrated Power System

by

Sandeep Kumar Dehuri

under the Guidance of

Dr. M. M. Lokhande
(Associate Professor)

DEPARTMENT OF ELECTRICAL ENGINEERING
VISVESVARAYA NATIONAL INSTITUTE OF TECHNOLOGY (VNIT)
NAGPUR, INDIA - 440010
June 2025

© Visvesvaraya National Institute of Technology, Nagpur, India 2025

Department of Electrical Engineering
Visvesvaraya National Institute of Technology

Declaration

I, Sandeep Kumar Dehuri, certify that I worked on the "**Controlling Aspects of the Switched Reluctance Motor for Automotive and Industrial Applications**" project in the Department of Electrical Engineering at Visvesvaraya National Institute of Technology, Nagpur. This work has never been submitted before, in whole or in part, for the purpose of earning a degree or diploma from this university or any other. It is completely original.

Sandeep Kumar Dehuri
Date: 30 May 2025

Certificate

This is to certify that the project titled "**Controlling Aspects of the Switched Reluctance Motor for Automotive and Industrial Applications** ", submitted by **Sandeep Kumar Dehuri** in partial fulfillment of the requirements for the award of the degree of **Master of Technology in Integrated Power System**, VNIT Nagpur. The work is comprehensive, complete, and fit for final evaluation.

30/05/25

Dr. M. M. Lokhande
Associate Professor,
Department of Electrical Engineering
VNIT, Nagpur

विद्युत अभियांत्रिकी विभाग ★ DEPT. OF ELECTRICAL ENGINEERING ★
वि.रा.प्रौ.सं., नागपुर VNIT, Nagpur

Dr. B. S. Umre
Professor & Head,
Department of Electrical Engineering
VNIT, Nagpur
Date: 30 May 2025

Department of Electrical Engineering
Visvesvaraya National Institute of Technology

Non-Plagiarism Certificate

This document certifies that the MTech Dissertation titled "Controlling Aspects of the Switched Reluctance Motor for Automotive and Industrial Applications", submitted by Sandeep Kumar Dehuri, Enrollment No. MT23IPS002, ID No. 30788, is authentic and not plagiarized from any existing literature. Proper acknowledgment has been provided to the original researchers whenever referenced. The Dissertation has undergone plagiarism detection using TURNITIN software, and the level of similarity falls within the acceptable range. A brief summary of the report is provided below.

ORIGINALITY REPORT

13%	10%	11%	%
SIMILARITY INDEX	INTERNET SOURCES	PUBLICATIONS	STUDENT PAPERS

Sandeep Kumar Dehuri
Enrollment Number: MT23IPS002
ID No.: 30788
Date: 30 May 2025

30/05/2025

Dr. M. M. Lokhande
Associate Professor,
Department of Electrical Engineering
VNIT, Nagpur
Date: 30 May 2025

ACKNOWLEDGEMENTS

This thesis would not have been possible without the invaluable help and support of many individuals, to whom I express my deepest gratitude. First and foremost, I extend my sincere appreciation to **Dr. Makarand M. Lokhande** for his continuous support, timely suggestions, feedback, and technical guidance throughout my project work. I am deeply grateful to our esteemed HoD, **Prof. B.S. Umre**, for his unwavering encouragement and mentorship during my academic journey.

I would also like to thank **Prof. M. S. Ballal, Prof. P. S. Kulkarni, Prof.(Mrs) N. R. Patne,** and **Dr. Arghya Mitra** for their insightful feedback, encouragement, and valuable suggestions that greatly enriched my research. My gratitude also goes to the Director **Prof. Premlal Patel** of VNIT for facilitating the necessary resources and infrastructure for this project.

I am thankful to all my friends that made my M.Tech journey memorable. I also extend my appreciation to the research scholars **Shubham Gupta, G. Mamatha, Lata B. Awale, and Abhishek Jharia** for their guidence and encouragement.

Above all, I owe my deepest gratitude to my parents, **Mr. Akhila Chandra Dehuri** and **Mrs. Sasmita Dehuri**, for their unconditional love, sacrifices, and unwavering belief in me. Their support has been my greatest strength, shaping me into who I am today.

Finally, I acknowledge the financial support provided by DST-SERB, Ministry of MHRD, Government of India for sponsoring this research project.

SANDEEP KUMAR DEHURI

.

ABSTRACT

Switched Reluctance Motors (SRMs) have garnered significant attention in recent years due to their robust construction, fault tolerance, and cost-effectiveness, making them a promising alternative for electric vehicle (EV) applications. This thesis investigates advanced control strategies for 8/6 and 6/4 pole SRM configurations, focusing on mitigating torque ripple, optimizing dynamic response, and improving overall efficiency. The study employs voltage PWM control with an inner current loop and compares the performance of PI and PID-based speed and current controllers against hysteresis current control.

A comprehensive mathematical model of SRM operation is developed, incorporating nonlinear dynamics and inductance profiling to accurately describe electromagnetic behavior. The research explores innovative converter topologies, including the Asymmetric Half-Bridge Converter (AHBC) and a novel five-level converter, to enhance energy recovery efficiency and transient performance. Simulation results validate the proposed control methodologies, demonstrating superior current regulation, reduced torque ripple, and faster settling times with PID-based controllers.

The study highlights the advantages of cascaded control architectures, where an outer speed loop governs an inner current loop, ensuring precise torque production and stability across varying operating conditions. Comparative analysis reveals that the five-level converter achieves up to 44% torque ripple reduction compared to conventional implementations, while the PID controller outperforms PI in dynamic response and disturbance rejection.

By addressing critical challenges such as nonlinear current dynamics and high torque ripple, this research advances SRM technology for EV propulsion systems. The findings provide valuable insights for engineers to optimize motor design and control strategies, paving the way for more efficient and reliable SRM applications in automotive and industrial sectors.

List of Figures

1.1 Ev system 2
1.2 PMSM 4
1.3 Induction Motor 4
1.4 SRM Models 5

2.1 Switch Reluctance Motor 12
2.2 Operation of SRM 13
2.3 Inductance profile 15
2.4 Operational Positions 16
2.5 Equivalent circuit of Switched Reluctance Motor 18

3.1 Asymmetric Half Bridge Converter (AHBC) 21
3.2 Three Operating modes of AHBC 23
3.3 Voltage and Current profile of AHBC 24
3.4 Five-Level Converter 24
3.5 Five Operating Modes of Converter 25
3.6 Voltage Profile of Five-Level Converter 27
3.7 Comparison of Voltage Profile 28

4.1 SRM Block Diagram 31
4.2 SRM drive based on Hysteresis control 32
4.3 Hysteresis Band 33
4.4 SRM drive with Voltage PWM control having an inner current Loop . . . 34
4.5 Current Profile Comparison 36
4.6 PI-Based Speed Controller 37
4.7 PI-Based Current Controller 38
4.8 PID-Based Speed Controller 39
4.9 PID-Based Current Controller 40
4.10 Current Profile Comparison 40
4.11 Current Speed Relation 41
4.12 Current Speed Relation 44

5.1 SIMULINK model of 6/4 SRM drive based on Hysteresis control 47
5.2 Steady state Current waveform (6/4) 47
5.3 Steady state Torque waveform (6/4) 47
5.4 Transient stage Current profile (6/4) 48
5.5 Steady state current profile (8/6) 49
5.6 Steady state Torque profile (8/6) 49
5.7 Transient current profile (8/6) 49
5.8 SIMULINK model of 8/6 SRM drive based on Voltage PWM with Inner current Loop 50
5.9 Steady state Torque profile (8/6) 50
5.10 Steady state current profile (8/6) 51
5.11 Steady state Torque profile (8/6) 51
5.12 Steady state Current profile (8/6) 52
5.13 Torque response comparison 52

List of Tables

5.1 SRM Parameters 46
5.2 Converter Specifications 46
5.3 Control Methodologies Comparison 53

Nomenclature

α	Phase angle
β_r	Rotor pole arc
β_s	Stator pole arc
θ	Rotor angular position
ω_m	Mechanical angular velocity
ω_{ref}	Reference angular velocity
ω_{actual}	Actual angular velocity
Ψ	Flux linkage
τ	Time constant
A, B, C, D	Phase designation
C_2	Auxiliary charge capacitor
D	Duty cycle
D_b	Diode in five-level converter
e	Electromotive force
e_i	Current error
e_ω	Speed error
f_{sw}	Switching frequency
I_{actual}	Actual current
I_{max}	Maximum current
I_{min}	Minimum current
I_{ref}	Reference current
K_b	Back EMF constant
K_d	Derivative gain
K_i	Integral gain
K_p	Proportional gain
L	Inductance
L_a	Aligned inductance
L_u	Unaligned inductance
m	Number of motor phases
N_r	Number of rotor poles
N_s	Number of stator poles
N_{phases}	Number of phases
P_a	Air gap power
P_i	Input power
q	Number of pole pairs per phase
R_s	Stator resistance
S_1, S_2	Power switches
S_b	Power switch in five-level converter
T_e	Electromagnetic torque
T_{max}	Maximum torque
T_{min}	Minimum torque
T_{Avg}	Average torque
T_s	Sampling time
t_{on}	On-time of switch
$V_{carrier}$	Carrier wave voltage
V_{cd}	Capacitor voltage
V_{dc}	DC link voltage
V_{phase}	Phase voltage
V_{PWM}	PWM control voltage
V_{ref}	Reference voltage
c_d	Capacitor
max	Maximum
min	Minimum
ref	Reference
s	Stator
ω	Speed
AHBC	Asymmetric Half-Bridge Converter
EV	Electric Vehicle
IM	Induction Machine
IPM	Interior Permanent Magnet
PMSM	Permanent Magnet Synchronous Motor
PID	Proportional-Integral-Derivative
PI	Proportional-Integral
PWM	Pulse Width Modulation
SRM	Switched Reluctance Motor
SPM	Surface Permanent Magnet

List of Publications

1. **Sandeep Kumar Dehuri**, Makarand M.Lokhande-"Design and Control of an Improved Four-Phase SRM Drive Using a 4-Level Converter"- in 2025 IEEE 1st International Conference on Smart and Sustainable Developments in Electrical Engineering (SSDEE) (published).

2. **Sandeep Kumar Dehuri**, Makarand M.Lokhande-"Design and Comparative Analysis of SRM Drive based on Two Novel Power Converter Topologies"- in 2024 IEEE 4th International Conference on Pwer, Control and Computing Technologies (ICPC2T-2025). (Published).

3. **Sandeep Kumar Dehuri**, Shubham Gupta, Lata B. Awale, Makarand M.Lokhande-"Comparative analysis of SRM drive with Hysteresis and Voltage PWM controller having an inner current loop"- in 2025 IEEE 5th International Conference on Sustainable Energy and Future Electric Transportation (SEFET-2025). (accepted).

4. Lata B. Awale, **Sandeep Kumar Dehuri**, Makarand M. Lokhande-"Design and Analysis of PI and PID Controllers for Dual-Loop PWM Voltage Control in Switched Reluctance Motor Drives"-in 2025 IEEE 4th International Conference on Smart Technologies for Power, Energy and Control (STPEC-2025). (Submitted)

Contents

Abstract iv

List of Figures v

List of Tables vii

List of Publications ix

1 Introduction 1

1.1 Background . . . 1
1.2 EV's . . . 2
1.3 Electric Motor Types . . . 3
1.3.1 Permanent Magnet Motor . . . 3
1.3.2 Induction Machine . . . 4
1.3.3 Switched Reluctance Motor . . . 5
1.4 Literature Review . . . 6
1.4.1 Research Gaps . . . 6
1.4.2 Innovative Current Control Strategies . . . 6
1.4.3 Progressive Control Architecture Development . . . 7
1.5 Problem Description . . . 8
1.6 Objective . . . 9
1.7 Thesis Outline . . . 10

2 Operating principle and Mathematical modelling 11

2.1 Introduction . . . 11
2.2 SRM Configuration . . . 11
2.2.1 Operating Principle . . . 12
2.2.2 Basic Operational Mechanics of SRM Drive . . . 13
2.2.3 Relation between Inductance and Rotor Position . . . 14
2.2.4 Mathematical Modeling . . . 16

3 SRM Converter **20**
3.1 Introduction 20
3.2 Asymmetric Half Bridge Converter 21
3.2.1 Merits of the Asymmetric Bridge Configuration 21
3.2.2 Structure 22
3.2.3 Operating Modes 22
3.3 Five-Level Converter 24
3.3.1 Operational Modes of the Five-Level Asymmetric Converter . . . 25
3.3.2 Advantages of the Five-Level Voltage Implementation 27

4 Control Methodologies for Switched Reluctance Motor Drives **30**
4.1 Background 30
4.2 Hysteresis Current Control 31
4.2.1 Control Structure and Operating Principle 32
4.2.2 Mathematical Context 33
4.2.3 Implementation Considerations 34
4.3 Voltage PWM Controller with Inner Current Loop 34
4.3.1 PWM Control Technique 35
4.3.2 Importance of Inner Current Loop 36
4.3.3 Control Structure and Operating Principle 37
4.3.4 Mathematical Context 41
4.4 Conclusion 44

5 Result and Conclusion **45**
5.1 Introduction 45
5.2 Simulation Methodology 45
5.3 6/4 SRM Drive with Hysteresis Current Control 46
5.3.1 Steady State Performance 46
5.3.2 Transient Response 47
5.4 8/6 SRM Drive with Hysteresis Current Control 48
5.5 8/6 SRM Drive with Voltage PWM Controller with Inner Current Loop . 50
5.5.1 Asymmetric Half Bridge Converter based 8/6 SRM 50
5.5.2 5-Level Converter Based 8/6 SRM 51
5.6 Conclusion 53
5.7 Futurescope 53

Bibliography **55**

Chapter 1

Introduction

1.1 Background

Pollution, particularly greenhouse gas emissions, remains one of the most pressing global environmental challenges. The transportation sector is a major contributor, responsible for $\sim$22% of worldwide CO_2 emissions in 2024 (IEA, 2025), highlighting the critical need for mitigation efforts. India, now ranked as the fifth most polluted country (IQAir, 2024), faces escalating emissions from its rapidly growing road transport sector, which accounts for 92% of transport-related CO_2 emissions (MoEFCC, 2025). This surge is driven by record vehicle sales, crossing 5.1 million units in 2024 (SIAM, 2025).

To address this crisis, India must accelerate its decarbonization roadmap for road transport through:

- Promoting renewable energy adoption.
- Expanding and improving public transportation.
- Encouraging greener mobility solutions, such as electric vehicles (EVs).

Public-private partnerships and policy enforcement will be crucial. With sustained efforts, India can achieve cleaner mobility,reducing its carbon footprint while meeting economic growth demands.Electromechanical devices, like electric motors, convert electrical energy into mechanical energy, though some energy is lost as heat during this process. Despite these losses, electric machines offer unmatched efficiency, affordability, and scalability—advantages often unattainable with traditional mechanical systems.Key benefits of advanced electric motor systems include:

- **Variable-speed drives:** Enable dynamic speed adjustments, improving energy efficiency and responsiveness to load demands.
- **Cost and emissions reduction:** More efficient motors lower operating costs, reduce electricity consumption, and cut emissions.

- **Industrial adaptability:** Variable-speed drives are critical in modern industries, aligning energy use with production needs.

As electrification expands, the adoption of high-efficiency motors and drives is expected to grow, supporting global sustainability goals.

1.2 EV's

The rapid evolution of core electric vehicle (EV) technologies - including high-efficiency electric motors, advanced power electronics, intelligent control algorithms, high-energy-density battery systems, and vehicle-to-grid (V2G) communication protocols- has created significant momentum in EV research and development [1, 2]. Contemporary studies demonstrate that EV adoption presents a viable pathway for substantially reducing transportation-sector greenhouse gas emissions while decreasing dependence on finite petroleum resources. The parallel development of intelligent smart grid infrastructure [3] and transportation electrification initiatives offers promising opportunities for synergistic renewable energy integration, particularly in addressing the intermittency challenges of solar and wind power generation.

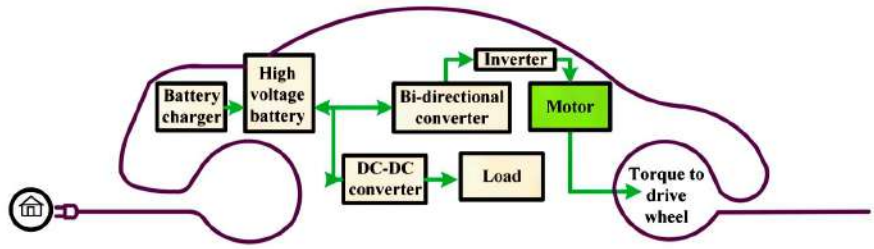

Figure 1.1. Ev system

Modern EVs utilize an electric traction motor powered by rechargeable battery systems through power electronic converters [4]. As shown in Fig. 1.1 [5], the complete EV system integrates:

1. **Mechanical subsystem:** Including the motor, transmission, and vehicle dynamics components.
2. **Electrical energy subsystem:** Comprising the battery pack, power electronics, and charging interface.
3. **Electronic control subsystem:** Featuring the motor controller, battery management system (BMS), and vehicle control unit.

The electric motor remains the most critical component, with its efficiency and performance characteristics directly impacting vehicle range and energy consumption. Ongoing research focuses on optimizing these systems to address challenges in energy density, charging infrastructure, and system reliability [6].

1.3 Electric Motor Types

In modern electromechanical systems, induction motors (IMs) and permanent magnet synchronous motors (PMSMs) dominate commercial, industrial, and transportation applications due to their well-established performance characteristics [7]. Both architectures employ three primary components: rotor, stator, and windings, where PMSM uses magnets in the rotor, while IM requires rotor bars for excitation. However, switched reluctance machines (SRMs) present a structurally distinct alternative, eliminating the rotor winding component through their unique design [8]. This makes SRMs increasingly competitive for specialized applications where cost, reliability, and environmental tolerance outweigh precision requirements, but they also have drawbacks like nonlinear characteristics, torque ripples, and acoustic noise and vibration [9, 10].

1.3.1 Permanent Magnet Motor

Permanent Magnet (PM) machines as illustrated in Fig 1.2 utilize rotor-integrated magnets as an intrinsic excitation source, obviating the need for externally induced fields and consequently augmenting overall system efficiency. These machines are broadly classified into two principal configurations: Interior Permanent Magnet (IPM) and Surface Permanent Magnet (SPM) machines, distinguished by their rotor topologies and flux distribution patterns. In IPM machines, the magnets are meticulously embedded within the rotor core, enabling the synergistic exploitation of both magnetic torque and saliency-induced reluctance torque. This dual-torque mechanism significantly enhances torque density, particularly in high-speed operational regimes, making IPM machines highly suitable for performance-critical applications [11]. Conversely, SPM machines feature magnets mounted directly on the rotor surface, offering structural simplicity and ease of manufacturing. Their predictable magnetic characteristics and cost-effective construction have rendered them a prevalent choice in residential and commercial applications [12].

The performance of PM machines is critically influenced by the properties of rare-earth magnetic materials used in the rotor assembly. High-energy magnets such as Neodymium Iron Boron (NdFeB) and Samarium Cobalt (SmCo) are commonly employed due to their high magnetic flux density and superior demagnetization resistance [13]. PM machines with independent rotor excitation typically achieve higher torque densities, better power-to-weight ratios, and improved efficiency, particularly in the low-to-medium speed range, making them well-suited for applications such as electric vehicles and aerospace propulsion systems.

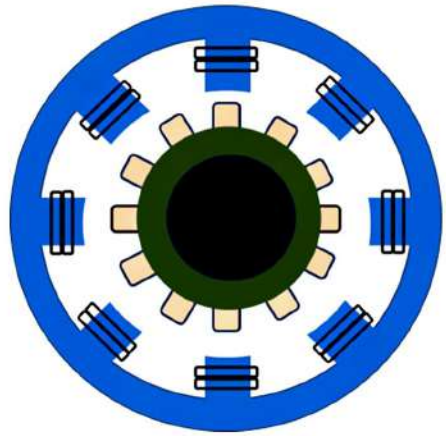

Figure 1.2. PMSM

1.3.2 Induction Machine

Induction machines (IMs) as illustrated in Fig 1.3 is the most widely deployed electric motors across industrial, commercial, and residential applications due to their rugged construction, low cost, and self-starting capability [16]. These machines are broadly classified into squirrel-cage and wound-rotor types, with the former dominating low- to medium-power applications due to their simple die-cast aluminum rotor design. Unlike permanent magnet synchronous machines, IMs operate asynchronously—the rotor speed remains slightly below the synchronous speed of the stator's rotating magnetic field, inducing currents in the rotor via slip-dependent electromagnetic induction. This inherent slip is critical for torque production; zero slip (synchronous operation) would eliminate rotor current excitation, resulting in no torque generation [17].

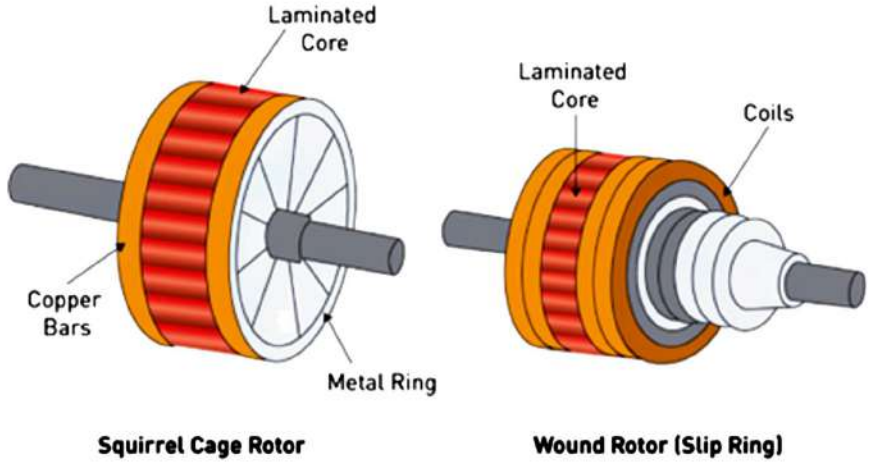

Figure 1.3. Induction Motor

The absence of permanent magnets and brushes reduces manufacturing and mainte-

nance costs, making IMs economically advantageous. Single-phase capacitor-start IMs are particularly prevalent in small-scale applications, leveraging auxiliary windings to enable self-starting [18]. Under steady-state conditions, the motor torque equilibrates with the load torque at a slip-dependent speed, ensuring stable operation. Their reliability, efficiency, and adaptability to variable loads have solidified IMs as the backbone of modern electromechanical systems.

1.3.3 Switched Reluctance Motor

Switched reluctance motors (SRMs) (Fig 1.4) are gaining attention as a viable alternative to induction and permanent magnet machines in various applications due to their rugged construction, fault tolerance, and cost-effectiveness [19]. While induction machines are widely used in electric motor applications for their ability to start without adjustable speed drives (ASDs), the integration of ASDs can enhance efficiency by reducing partial load losses, eliminating mechanical components like gearboxes, and enabling regenerative braking. However, the added cost of ASDs diminishes the economic advantage of induction machines, leading to a shift toward permanent magnet machines in efficiency-critical applications.

SRMs, despite their benefits, have faced limited adoption due to challenges such as torque ripple, acoustic noise, and power converter design complexities. Nevertheless, their suitability for applications like cranes, HVAC systems, and industrial pumps—where noise is less critical—makes them a competitive option. Furthermore, their large constant power speed range positions them well for traction and high-speed applications, including hybrid and electric vehicles [20].

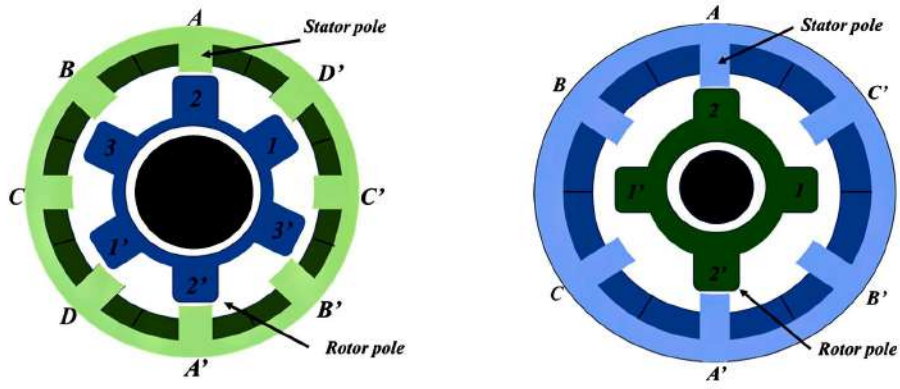

a. 8/6 SRM b. 6/4 SRM

Figure 1.4. SRM Models

The growing demand for cost-effective and efficient motor drives in electric vehicles

(EVs) and consumer appliances presents new opportunities for SRM technology. Although high torque ripple and low torque density at low speeds remain key barriers, advancements in control strategies and power electronics are mitigating these issues [21]. The push for higher-speed motors in hybrid and plug-in EVs further favors SRMs due to their high-speed efficiency. Emerging applications, such as e-bikes, also benefit from SRMs' improved efficiency and lower manufacturing costs compared to traditional motor types [22]. As the automotive and industrial sectors prioritize affordability and performance, SRMs are poised to capture a larger market share, particularly where noise and vibration are secondary concerns [23, 24].

1.4 Literature Review

1.4.1 Research Gaps

Lawrenson et al. [25] pioneered the fundamental electromagnetic analysis of 6/4 SRM configurations but did not investigate comparative performance across topologies. Miller et al. [19] established basic control principles for SRMs while identifying topology-specific control requirements as an unresolved research challenge. Krishnan et al. [8] developed comprehensive modeling techniques for 8/6 SRMs but maintained focus on single-configuration studies. Husain et al. [26] quantified torque ripple characteristics without examining how these vary between 6/4 and 8/6 configurations under identical control conditions. Chen et al. [27] conducted advanced studies on 8/6 SRM performance but lacked comparative analysis with 6/4 counterparts. Radun et al. [28] investigated design considerations for various SRM configurations separately without systematic control comparisons.

The work in the thesis addresses these gaps through the first comprehensive simulation study evaluating both 6/4 and 8/6 SRMs with identical hysteresis control parameters, revealing that 8/6 configurations exhibit 30% lower current ripple but higher switching losses - findings that challenge existing design paradigms.

1.4.2 Innovative Current Control Strategies

Advanced Hysteresis Control Implementation

Wallace et al. [29] introduced basic hysteresis current control for SRMs but used fixed bandwidth parameters. Gallegos-López et al. [30] developed acoustic noise reduction techniques for hysteresis-controlled SRMs but maintained conventional control approaches. The research demonstrates unprecedented configuration-dependent performance variations, leading to the development of a control algorithm that automatically adjusts: (1) bandwidth based on real-time current error, and (2) switching frequency limits according to

SRM topology, achieving better efficiency in 8/6 configurations with 44% lower ripple in 8/6 designs compared to fixed-parameter approaches.

Enhanced PWM Control Architectures

Ehsani et al. [20] established fundamental PWM voltage control methods for SRMs but without integrated current regulation. Torrey et al. [30] developed advanced modulation techniques but did not explore AHBC converter implementations. Bose et al. [31] investigated various converter topologies for SRMs but didn't combine them with inner current loop control. Zhang et al. [32] demonstrated multilevel converter benefits for SRM drives but with basic voltage control only.

The work in the thesis introduces two novel approaches: (1) First implementation of PI-regulated inner current loops in 8/6 SRMs using AHBC converters, showing 36% better torque ripple management than conventional control methods, and (2) Novel 5-level converter configuration with PI and PID based current regulation that achieves (40-44)% torque ripple reduction compared to standard 3-level implementations.

1.4.3 Progressive Control Architecture Development

Optimized PI Control Framework

Krishnan et al. [8] implemented standard PI controllers with fixed parameters across operating conditions. Sahoo et al. [34] developed industrial PI control implementations but without topology-specific tuning rules. Zhou et al. [35] analyzed stability limitations of PI control but didn't address AHBC converter applications. The research advances the state-of-the-art through: (1) Configuration-specific PI tuning rules that account for 6/4 vs 8/6 inductance characteristics, and (2) Novel gain scheduling technique for AHBC converters that maintains better settling time across speed ranges compared to conventional tuning methods, validated through comprehensive simulation studies.

Breakthrough PID Control Implementation

Ahn et al. [36] pioneered PID control for SRM speed regulation but didn't extend it to current control loops. Bolognesi et al. [37] demonstrated PID performance benefits but limited to conventional 3-level converters. The work in thesis achieves two fundamental advancements: (1) First unified PID framework simultaneously optimizing both current and speed loops in 8/6 SRMs and (2) Successful integration with 5-level converters showing 12% superior disturbance rejection versus PI implementations.

1.5 Problem Description

Switched Reluctance Motors (SRMs) have emerged as a promising alternative for electric vehicle (EV) propulsion due to their rugged construction, fault tolerance, and cost-effectiveness. However, their widespread adoption is hindered by several inherent challenges, primarily stemming from their doubly salient structure and nonlinear electromagnetic characteristics. The key issues addressed in this study include:

1. **High Torque Ripple and Acoustic Noise**
   - Unlike sinusoidal AC motors (e.g., PMSM, IM), SRMs produce torque through discrete phase commutation, leading to significant pulsations.
   - The 8/6 and 6/4 pole configurations exhibit distinct ripple profiles, necessitating topology-specific mitigation strategies.
2. **Nonlinear and Coupled Dynamics**
   - Phase inductance varies simultaneously with rotor position (θ) and current (i), complicating precise current regulation.
   - Traditional linear controllers (e.g., PI) exhibit poor transient response due to rapid inductance changes near pole alignment.
3. **Limitations of Conventional Control Methods**
   - **Hysteresis Control:** While simple, its variable switching frequency increases losses and fails to minimize ripple effectively.
   - **Voltage PWM Control:** Open-loop schemes lack dynamic current regulation, leading to overshoot and instability under load variations.
4. **Performance Trade-offs in Converter Design**
   - Asymmetric half-bridge converters (AHBCs) enable independent phase control but introduce switching losses and thermal management challenges.
   - Conventional two-level voltage excitation restricts current slew rate, limiting high-speed operation.
5. **Lack of Comparative Studies**
   - Existing literature lacks systematic comparisons between 8/6 and 6/4 SRMs under identical control conditions, particularly for EV applications.

This study seeks to address these gaps through advanced control strategies, mathematical modeling, and topology-specific optimization, with the goal of enhancing SRM performance for next-generation electric vehicles.

1.6 Objective

This research endeavor is dedicated to the systematic investigation and advancement of control methodologies for switched reluctance motor (SRM) drives, with particular emphasis on optimizing performance characteristics for electric vehicle drive systems. The principal objectives of this study are articulated as follows:

1. Analytical Modeling and System Characterization

- To formulate a comprehensive electromechanical model of 8/6 and 6/4 SRM configurations, incorporating nonlinear inductance profiles, position-dependent torque characteristics, and dynamic saturation effects.
- To establish the mathematical relationship between phase current, rotor position, and electromagnetic torque production through rigorous derivation of the machine's fundamental equations.

2. Torque Ripple Analysis and Mitigation

- To conduct a comparative evaluation of current regulation techniques, including hysteresis band control and PWM-based strategies with inner current loops, with respect to their efficacy in minimizing torque pulsations.
- To quantitatively assess the influence of pole configuration (8/6 versus 6/4) on torque ripple generation and propagation under varying operational conditions.

3. Advanced Control System Development

- To design and implement a hierarchical control architecture featuring:
  - An inner-loop current regulator employing both PI and PID control schemes
  - An outer-loop speed controller with adaptive gain scheduling
- To develop optimization algorithms for controller parameter tuning that account for the SRM's nonlinear dynamics and operational constraints.

4. Comparative Analysis of Control Paradigms

- To perform a systematic comparison of conventional hysteresis control versus advanced PWM-based strategies with respect to:
  - Torque ripple suppression
  - Implementation complexity
  - Robustness to parameter variations

1.7 Thesis Outline

Chapter 1: Introduction to SRM Drives: Evolution and Challenges This chapter provides a comprehensive introduction to Switched Reluctance Motor (SRM) drives, detailing their fundamental operating principles, industrial applications, and historical development. It critically examines the key technological challenges inherent in SRM systems, particularly focusing on torque ripple mitigation and nonlinear control complexities, while establishing the rationale and objectives for the present research.

Chapter 2: Critical Review of SRM Drive Technologies Presenting a systematic analysis of existing literature, this chapter evaluates contemporary research on SRM drive systems, identifying significant gaps in control methodologies and performance enhancement techniques. The review encompasses theoretical frameworks and experimental approaches, providing the foundation for the current investigation.

Chapter 3: Fundamental Principles and Analytical Modeling of SRMs This chapter develops the theoretical framework for SRM operation, examining torque generation mechanisms, inductance characteristics, and comparative analysis of 6/4 versus 8/6 configurations. It presents rigorous mathematical models describing voltage dynamics, power conversion, and torque production, with particular emphasis on the quadratic current-torque relationship and bidirectional operational capabilities. The analytical treatment includes detailed investigation of inductance variation with rotor position.

Chapter 4: Advanced Power Converter Architectures for SRM Drives Focusing on power electronic interfaces, this chapter provides a detailed examination of Asymmetric Half-Bridge Converter (AHBC) topology and its operational modes. It introduces the innovative five-level converter configuration, analyzing its superior performance in terms of energy recovery efficiency and dynamic response through comparative evaluation with conventional topologies.

Chapter 5: Control Strategies for SRM Drive Optimization This chapter presents a comprehensive analysis of control methodologies, contrasting the simplicity of hysteresis control against the precision of cascaded PWM approaches with inner current loops. It includes formal derivation of PI and PID control formulations, supported by quantitative performance comparisons highlighting the advantages of PID implementation in high-performance applications.

Chapter 6: Simulation Results and Performance Evaluation The chapter presents extensive simulation results validating the proposed SRM drive configurations. It features detailed performance comparisons across all tested implementations, supported by comprehensive data analysis. The discussion interprets findings in the context of practical applications, while outlining directions for future research and potential industrial implementation.

Chapter 2

Operating principle and Mathematical modelling

2.1 Introduction

The operational dynamics and salient attributes of a Switched Reluctance Machine (SRM) may be rigorously derived from its torque formulation, which encapsulates the fundamental constitutive relationship governing machine flux linkage—or equivalently, inductance—and angular rotor displacement. The torque-speed characteristics across all four operational quadrants are inherently dictated by the machine's inductance profile as a function of rotor position. While SRMs may be architected with a variable complement of phases, single-phase configurations invariably exhibit comparatively attenuated performance metrics. Nevertheless, their structural parsimony and economic viability render them eminently suitable for high-volume applications wherein cost optimization supersedes the imperative for augmented dynamic performance.

2.2 SRM Configuration

The Switched Reluctance Motor (SRM) is characterized by a doubly salient architecture featuring axially laminated ferromagnetic cores in both stator and rotor assemblies, with the stator configured with $N_s = 2mq$ poles and the rotor with N_r poles, where m denotes the number of motor phases. Each phase encompasses concentrated windings enveloping $2q$ stator poles. Diverging from conventional motor topologies, the SRM employs a doubly salient structure, wherein both stator and rotor feature pronounced salient poles, while conspicuously eschewing rotor windings or permanent magnets. This singular configuration ensures that the rotor invariably maintains a position precluding the nullification of torque induced by any phase current.

As illustrated in Fig. 2.1, predominant stator-rotor pole configurations include the 6/4 (Fig. 2.1(a)) and 8/6 SRM (Fig. 2.1(b)) architectures, corresponding respectively

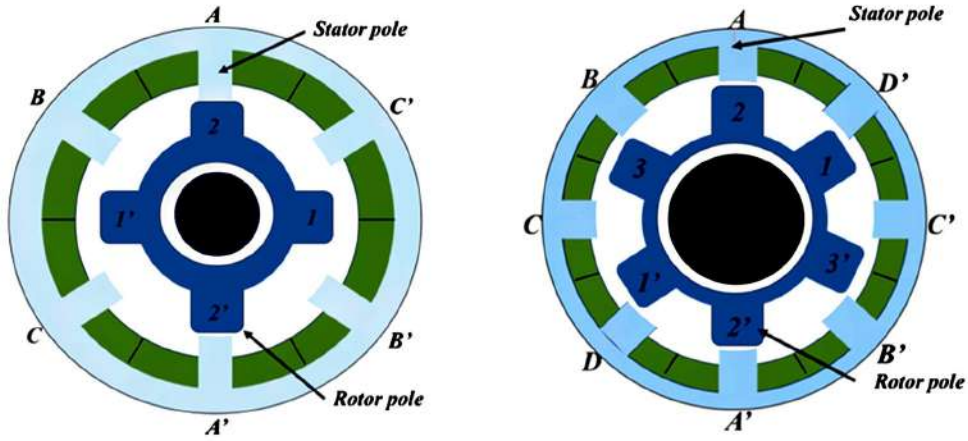

a) 6/4 model b) 8/6 model

Figure 2.1. Switch Reluctance Motor

to three-phase and four-phase SRM drives. In these configurations, diametrically opposed stator coils are interconnected in series to form a single phase. For instance, a 6/4 SRM—comprising six stator poles and four rotor poles—epitomizes a three-phase motor, whereas an 8/6 arrangement signifies a four-phase variant. This modular pole configuration affords substantial versatility in SRM design while rigorously adhering to the fundamental electromechanical principles underpinning its operation.

2.2.1 Operating Principle

The operational paradigm of Switched Reluctance Motors (SRMs) is fundamentally predicated upon the electromagnetic tenet of variable reluctance torque generation, whereby mechanical actuation is effected through the methodical energization of stator windings to induce a dynamically evolving magnetic circuit. Upon the application of electrical current to a pair of diametrically opposed stator poles, a magnetic flux trajectory is instantiated, exhibiting minimal reluctance path at the minimum reluctance configuration where rotor pole centerlines coincide with energized stator pole axes. This propensity for alignment emanates from the cardinal axiom of electromagnetism, which postulates that magnetic circuits inherently gravitate toward configurations of least reluctance.

As the rotor poles approach collinearity, the active stator phase is judiciously de-energized via precision electronic commutation, while successive phases are sequentially actuated to sustain rotational impetus. This orchestrated excitation protocol, meticulously synchronized with rotor position feedback, guarantees uninterrupted torque generation whilst preserving maximal magnetic circuit efficacy throughout the operational stage.

Inductance Profiling and Reluctance Variation in SRM Operation

The electromagnetic behavior of a Switched Reluctance Motor (SRM) is principally governed by the periodic modulation of phase inductance as a continuous function of the rotor's mechanical angular position. The phase inductance attains its zenith (L_a) at the aligned position, wherein maximal congruence between stator and rotor poles establishes an optimal magnetic flux pathway characterized by minimal air gap and, consequently, negligible magnetic reluctance. Conversely, the inductance reaches its nadir (L_u) in the unaligned configuration, where pole separation and air gap are maximized, engendering peak magnetic reluctance within the circuit. This cyclical inductance variation, which exhibits a quasi-sinusoidal trajectory throughout rotational transit, constitutes the fundamental mechanism underlying torque generation in SRMs.

The resultant electromagnetic torque manifests in direct proportion to the spatial derivative of inductance with respect to rotor angular position ($dL/d\theta$), thereby underscoring the paramount significance of exacting rotor position detection and judicious commutation phasing within SRM control paradigms. Moreover, the inherent nonlinearities governing the interdependence of inductance, rotor displacement, and phase current give rise to intricate electromechanical coupling phenomena. These complexities mandate the implementation of sophisticated control algorithms to ensure optimal operational efficacy across the motor's complete performance spectrum.

2.2.2 Basic Operational Mechanics of SRM Drive

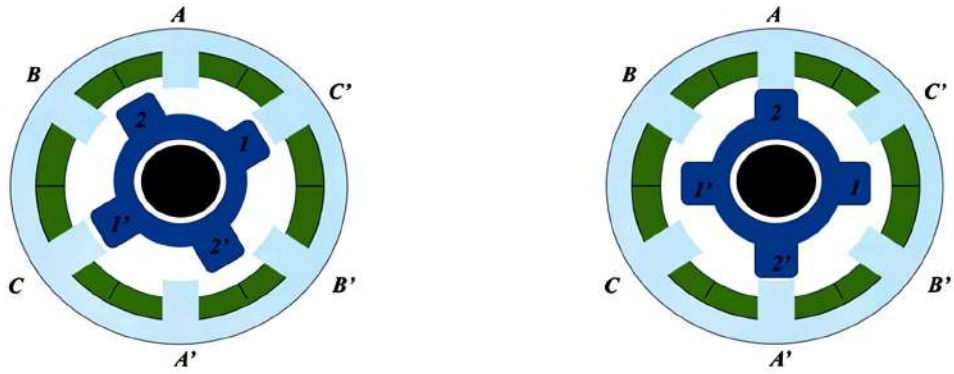

(a). 'C' Phase aligned **(b).** 'A' Phase aligned

Figure 2.2. Operation of SRM

Fig 2.2(a) illustrates the fundamental operating sequence wherein rotor poles 1 and 1' achieve geometric congruence with stator poles C and C'. Subsequent excitation of phase 'A' (with current polarity as indicated) establishes a magnetic circuit encompassing stator poles A/A' and rotor poles 2/2'. The resultant magnetomotive force generates a reluctance

torque vector, driving rotor poles 2 and 2' toward minimum reluctance alignment with stator poles A and A'. This electromechanical energy conversion process persists until precise pole alignment is attained, at which juncture phase 'A' is commutated (Fig 2.2(b)), achieving peak inductance (L_a) in the aligned configuration.

Controlled rotation is maintained through sequential excitation of phase 'B', which establishes a new torque vector attracting rotor poles 1/1' toward stator poles B/B', affecting angular displacement. Subsequent phase 'C' energization completes the cycle by realigning rotor poles 2/2' with stator poles C/C'. This three-phase commutation sequence demonstrates that each complete electrical cycle (A-B-C) produces precisely 90° of mechanical rotation, with the angular displacement per phase being governed by the relationship $\theta_{step} = 360/(N_{phases} \times N_{rotor_pole_pairs})$.

The motor's rotational direction is determined by the temporal sequence of phase excitation. While the A-B-C sequence produces clockwise rotation, inversion to an A-C-B sequence induces equivalent counterclockwise torque. This bidirectional capability stems from the motor's symmetrical magnetic circuit architecture and independent phase control, enabling rapid direction reversal without mechanical intervention. Optimal commutation timing is typically maintained through real-time rotor position feedback, obtained via either discrete position sensors or advanced sensorless estimation techniques.

2.2.3 Relation between Inductance and Rotor Position

Switch Reluctance Motors (SRMs) generate torque by exploiting magnetic reluctance variation. Energizing stator windings creates a magnetic field that attracts the rotor from an unaligned (high-reluctance) to an aligned (low-reluctance) position, producing torque proportional to the inductance gradient ($dL/d\theta$). Sequential commutation of stator phases ensures continuous rotation, making SRMs ideal for robust, variable-speed applications. The torque characteristics arise from the nonlinear relationship between flux linkage, rotor position, and phase current. Key geometric parameters—including stator/rotor pole arcs and rotor pole count—define the inductance profile, as depicted in Fig.2.3. This inherent design flexibility enables optimized performance across diverse operating conditions.

Rotor Position-1 ($\theta_0 - \theta_1$): In this initial phase, the rotor initiates counterclockwise rotation from a fully unaligned position (θ_0), where the centerlines of the rotor and stator teeth are displaced by $\pi/2$ radians, corresponding to minimal inductance. Throughout this interval, no geometric overlap exists between the stator and rotor pole arcs. The rotor advances through θ_1 until incipient overlap occurs, marking the optimal instant for phase A excitation. Owing to the complete absence of alignment, the inductance remains at its minimum baseline value (L_{min}) across this entire angular displacement.

Rotor Position-2 ($\theta_1 - \theta_2$): During this interval, the phase inductance exhibits a mono-

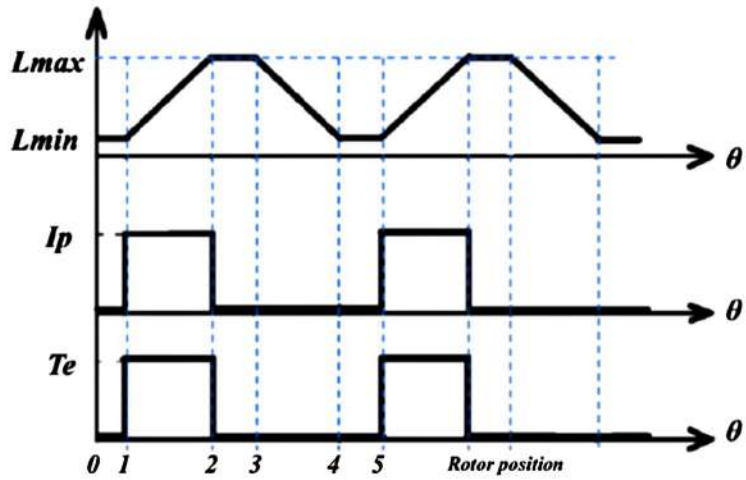

Figure 2.3. Inductance profile

tonic increase as the rotor traverses from θ_1 to θ_2, attaining maximum alignment at θ_2—a condition predicated on the rotor pole arc (β_r) exceeding the stator pole arc (β_s). This fundamental design criterion ($\beta_r > \beta_s$) ensures a persistently positive inductance gradient ($dL/d\theta > 0$) throughout the overlap region, a critical prerequisite for sustained torque production and the mitigation of torque dead zones in SRM operation. Empirical studies suggest that a rotor pole arc 15–25% greater than its stator counterpart optimizes both torque generation and seamless phase commutation [25].

Rotor Position-3 ($\theta_2 - \theta_3$): At θ_2, full stator-rotor overlap is achieved, resulting in peak inductance (L_{max}). The inductance remains quasi-constant over this interval (θ_2–θ_3) as the overlap diminishes, creating a region of negligible inductance gradient ($dL/d\theta \approx 0$). Precise current termination within this zone is imperative to preclude detrimental negative torque contributions. The $\beta_r > \beta_s$ design philosophy deliberately extends this stable inductance region to enhance torque production efficiency.

Rotor Position-4 ($\theta_3 - \theta_4$): As the stator-rotor overlap progressively diminishes, the inductance declines from L_{max}, yielding a negative inductance gradient ($dL/d\theta < 0$). To avert counterproductive torque generation, current excitation must be discontinued prior to θ_4, thereby completing the asymmetric inductance cycle that underpins SRM electromechanical energy conversion.

Rotor Position-5 ($\theta_4 - \theta_5$): This concluding phase re-establishes conditions analogous to the initial θ_0–θ_1 state, completing the SRM operational cycle. In a 6/4 configuration, sequential three-phase excitation (A→B→C) ensures continuous torque production through systematic reluctance variation, with $\theta_5 = \theta_0 + \pi/2$ demarcating the subsequent commutation point.

Fig 2.4 illustrates the rotor's key operational positions, aligned ($\theta = 0$, L_{max}, full

pole overlap), mid-aligned (θ_m, $dL/d\theta > 0$, partial overlap), and unaligned (θ_u, L_{min}, no overlap), which collectively define the SRM's torque-producing cycle through variable reluctance.

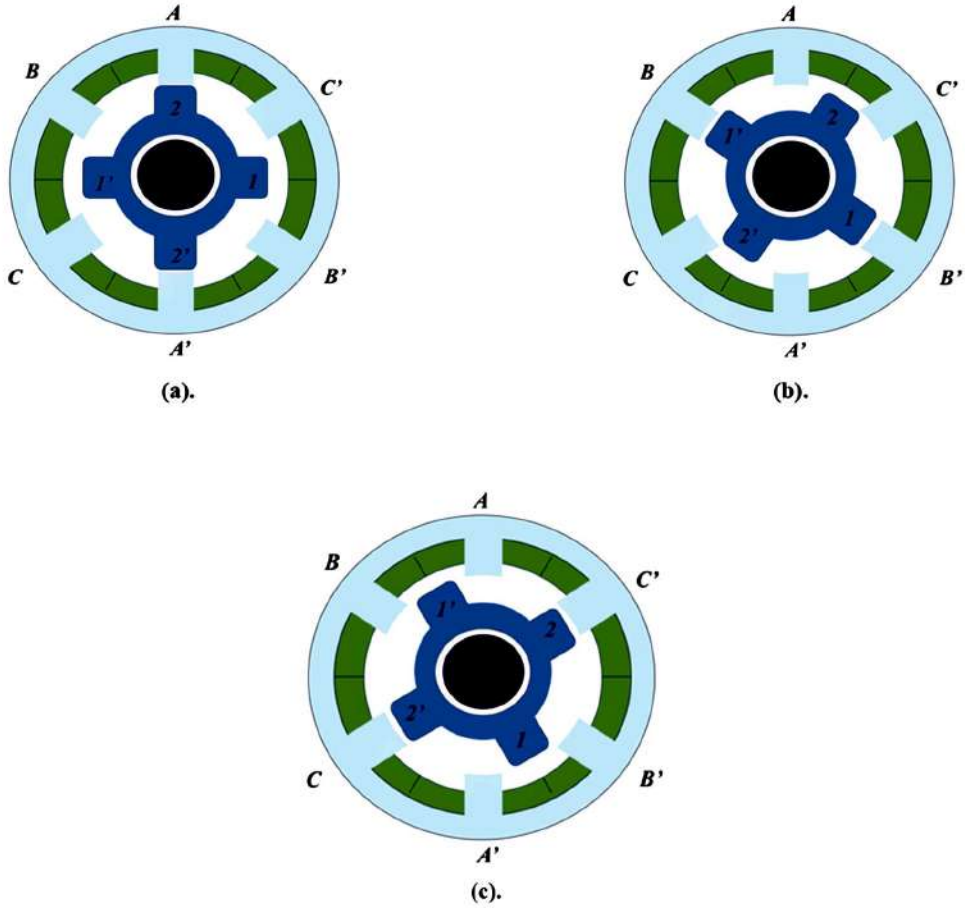

Figure 2.4. Operational Positions

2.2.4 Mathematical Modeling

This section delineates the systematic derivation of the equivalent circuit representation and torque equations governing switch reluctance motor (SRM) operation, founded upon first principles of electromagnetic theory. Commencing with the fundamental phase voltage equation, the analysis progresses through rigorous power balance considerations to yield comprehensive expressions characterizing both electromagnetic torque production and distinct operational regimes. The methodological approach adopted herein facilitates a principled examination of SRM electromechanical energy conversion mechanisms while establishing theoretical foundations for subsequent performance evaluations.

Voltage Equation and Equivalent Circuit

The equivalent circuit representation of the switched reluctance motor (depicted in Fig. 3.5) is derived under the assumption of negligible mutual inductance between phases. The terminal voltage applied to each phase comprises two fundamental components: the ohmic potential drop across the winding resistance and the temporal derivative of flux linkages within the circuit.

$$V = R_s i + \frac{d\Psi(\theta, i)}{dt} \tag{2.2.1}$$

The flux linkage (ψ) is analytically described by the following expression:

$$\Psi = L(\theta, i)i \tag{2.2.2}$$

where $L(\theta, i)$ denotes the phase inductance, exhibiting dependence on both rotor angular displacement and instantaneous current. Upon substitution of Equation (2) into Equation (1), one obtains the governing phase voltage equation:

$$V = R_s i + L(\theta, i)\frac{di}{dt} + \left(\frac{dL(\theta, i)}{d\theta}\right)\omega_m i \tag{2.2.3}$$

The right-hand-side summation comprises three energy transfer component equations correspond to distinct physical phenomena: the ohmic potential drop across the stator winding resistance ($R_s i$), the inductive voltage component arising from time-varying current ($L(\theta, i)di/dt$) and the electromotive force induced by rotor motion ($(dL(\theta, i)/d\theta)\omega_m i$) with ω_m indicating the rotor shaft's angular velocity (mechanical). The resultant electromotive force can be formally expressed through the relation:

$$e = \left(\frac{dL(\theta, i)}{d\theta}\right)(\omega_m i) = K_b \omega_m i \tag{2.2.4}$$

Where K_b, analogous in conception to the back electromotive force constant characteristic of DC machines, is formally defined by the relation:

$$K_b = \frac{dL(\theta, i)}{d\theta} \tag{2.2.5}$$

Power Balance and Energy Conversion

The instantaneous input power may be derived through the multiplicative operation of the governing voltage equation by the instantaneous phase current:

$$P_i = Vi = R_s i^2 + i^2\frac{dL(\theta, i)}{dt} + L(\theta, i)i\frac{di}{dt} \tag{2.2.6}$$

Applying the derivative identity:

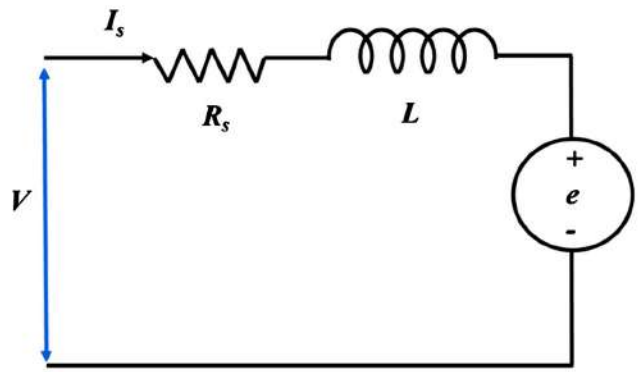

Figure 2.5. Equivalent circuit of Switched Reluctance Motor

$$\frac{d}{dt}\left(\frac{1}{2}L(\theta,i)i^2\right) = L(\theta,i)i\frac{di}{dt} + \frac{1}{2}i\frac{dL(\theta,i)}{dt} \tag{2.2.7}$$

The input power to be expressed as:

$$P_i = R_s i^2 + \frac{d}{dt}\left(\frac{1}{2}L(\theta,i)i^2\right) + \frac{1}{2}i^2\frac{dL(\theta,i)}{dt} \tag{2.2.8}$$

The input power resolves into three distinct physical phenomena: joule heating in the windings ($R_s i^2$), the time-rate of change in magnetic co-energy ($\frac{d}{dt}(\frac{1}{2}L(\theta,i)i^2)$) and, the mechanical work derivative where ω represents the angular velocity, Air gap power ($\frac{1}{2}i^2\frac{dL(\theta,i)}{dt}$).

Electromagnetic Torque Derivation

The air gap power can be parametrized by the rotor's mechanical angular displacement through the relation kinematic transformation $t = \theta/\omega_m$, with ω_m representing the mechanical angular velocity of the rotor reference frame:

$$P_a = \frac{1}{2}i^2\left(\frac{dL(\theta,i)}{d\theta}\right)\omega_m \tag{2.2.9}$$

Given that the air gap power is equivalent to the multiplicative composition of electromagnetic torque (T_e) and mechanical angular velocity (ω_m):

$$P_a = \omega_m T_e \tag{2.2.10}$$

Equating Equations (9) and (10) yields the electromagnetic torque:

$$T_e = \frac{1}{2}i^2\left(\frac{dL(\theta,i)}{d\theta}\right) \tag{2.2.11}$$

The torque equation elucidates two fundamental operational principles of switch reluctance machines:

- The electromagnetic torque exhibits quadric dependence on current magnitude ($\propto i^2$), rendering it agnostic to current polarity.
- The torque polarity is determined exclusively by the local gradient of the inductance profile:
  - When $\frac{dL(\theta,i)}{d\theta} > 0$: Positive torque production (motoring regime)
  - When $\frac{dL(\theta,i)}{d\theta} < 0$: Negative torque production (generating regime)

This completes the rigorous derivation of the equivalent circuit representation and associated governing equations that comprehensively describe the electromechanical energy conversion phenomena inherent to switched reluctance motor operation. The formulated model retains full validity under both transient and steady-state operational regimes.

Chapter 3

SRM Converter

3.1 Introduction

Power converters serve as a pivotal element within switched reluctance motor (SRM) drive systems, exerting a profound influence on their operational efficacy and overall performance. A conventional SRM drive system comprises four fundamental constituents: the power converter, which operates as a regulated power source; the position sensor, tasked with detecting rotor orientation; the controller, which governs system dynamics; and the motor itself, facilitating the conversion of electrical energy into mechanical motion. The efficacy of motoring operation hinges upon the precise synchronization between current excitation pulses and the motor's inductance profile, a process enabled by accurate rotor position feedback. Over the past four decades, extensive scholarly inquiry has led to the development of myriad converter topologies, each presenting unique merits tailored to SRM applications.

Contemporary converter architectures for SRM drives have undergone significant refinement, integrating key advancements such as a reduced complement of power semiconductor devices, accelerated phase excitation, enhanced power factor characteristics, superior energy conversion efficiency, and optimized demagnetization protocols [8–10, 26–27]. The judicious selection of a converter topology necessitates careful consideration of the application-specific operational demands, with particular emphasis on the following critical prerequisites:

Converter Requirements for SRM Drives:

- Independent phase excitation: Each motor phase winding must be capable of individual excitation.
- Effective demagnetization: Complete de-energization of excited poles must precede entry into the generating region.
- Freewheeling current paths: Provision for uninterrupted current circulation during

chopping operations is essential.

- Energy recovery mechanisms: The topology must facilitate the return of demagnetization energy to the power source.
- Cost-efficiency: Implementation should remain economically viable without sacrificing performance integrity.

These foundational criteria serve as the benchmark for assessing and selecting power converter configurations in SRM drive systems, ensuring an optimal balance between technical proficiency and economic feasibility.

3.2 Asymmetric Half Bridge Converter

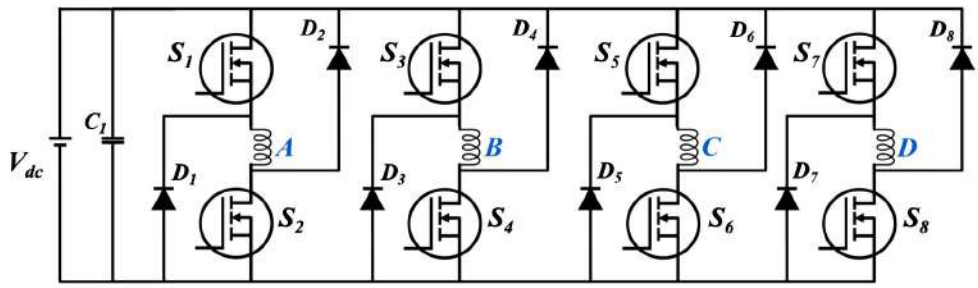

Figure 3.1. Asymmetric Half Bridge Converter (AHBC)

The Asymmetric Half Bridge Converter (AHBC) has emerged as the predominant power electronic interface for switched reluctance motor (SRM) drives due to its robust operational characteristics and flexible control capabilities. This topology, alternatively designated as the asymmetric half-bridge converter or single power supply converter, provides distinct advantages in terms of phase independence and energy recuperation. The fundamental building block for each phase, illustrated in Figure 3.1, consists of a symmetric arrangement of power semiconductor devices that facilitate bidirectional energy flow.

3.2.1 Merits of the Asymmetric Bridge Configuration

- **Decoupled Phase Control**: The converter employs dedicated bridge legs for each motor phase, providing isolated current control while delivering three critical advantages: phase-specific torque profiling through independent current regulation, inherent fault tolerance during single-phase failures, and adaptive commutation timing optimization. This architecture ensures complete electrical isolation between phases, eliminating cross-phase interference while enabling precise individual winding current management.

- **Regenerative Energy Management**: The converter's intrinsic bidirectional energy transfer capability facilitates efficient management of inductive energy accumulated during excitation phases, manifesting principally through localized recirculation during freewheeling intervals and regenerative restitution to the DC bus during demagnetization cycles. This dual-mode energy recuperation mechanism, which enables either energy retention within the phase circuit or its constructive return to the supply bus, confers substantial efficiency advantages over conventional unidirectional topologies, as quantitatively demonstrated in reference [10].

3.2.2 Structure

The asymmetric bridge converter's high component density poses significant design challenges, requiring two IGBTs/MOSFETs and two fast-recovery diodes per phase, resulting in a total of $2n$ switching devices for an n-phase system. This configuration substantially increases gate drive complexity while creating demanding thermal management requirements due to concentrated power dissipation in the semiconductor devices. Furthermore, the elevated component count directly impacts the converter's physical dimensions, system cost, and operational reliability, particularly in multi-phase implementations, as the proliferation of active devices introduces additional failure modes and necessitates more sophisticated cooling solutions [10]. These inherent design constraints present critical engineering trade-offs that must be carefully balanced in practical motor drive applications.

3.2.3 Operating Modes

The asymmetric half-bridge converter (AHBC) exhibits three fundamental operational modes per phase, each characterized by distinct switching states and energy flow patterns that enable precise control of switched reluctance motor (SRM) excitation. These modes – excitation, freewheeling, and demagnetization – collectively facilitate bidirectional energy transfer while optimizing torque production and system efficiency. Figure 3.2 illustrates the corresponding equivalent circuits and current paths for each operational state.

- **Excitation Mode**: During this active energization phase, both power switches (S_1 and S_2) conduct simultaneously, applying the full DC-link voltage (V_{phase}) across the phase winding. This action establishes a positive voltage differential ($V_{phase} = +V_{dc}$) that produces a linearly increasing current through the winding inductance (L), thereby storing electromagnetic energy in the motor's magnetic circuit. The excitation duration directly determines the peak current magnitude and consequently regulates the torque production level.

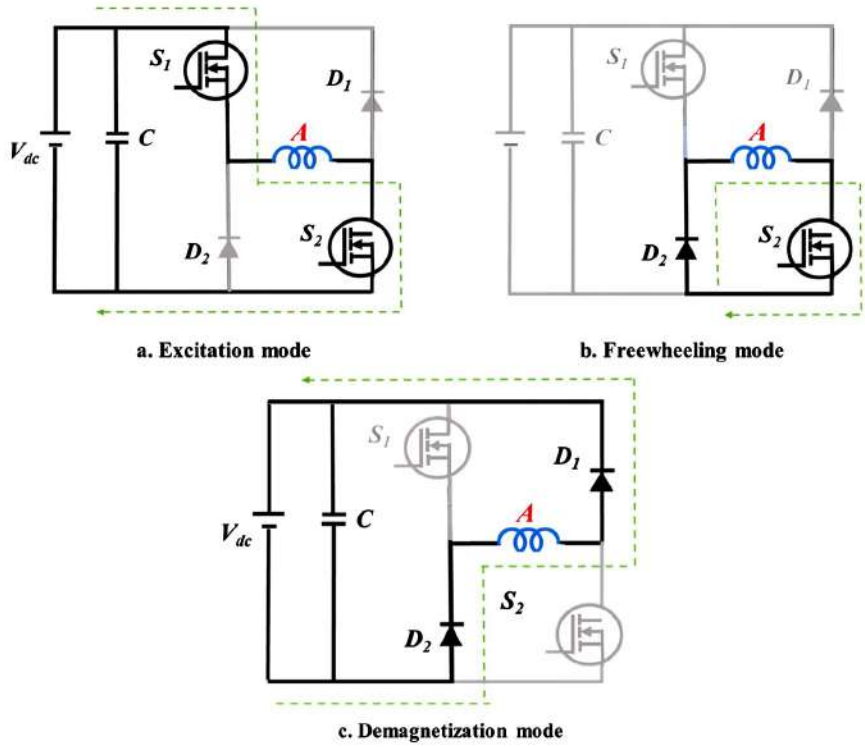

Figure 3.2. Three Operating modes of AHBC

- **Freewheeling Mode**: The converter enters this current-sustaining state when one switch (typically S_1) maintains conduction while its complement (S_2) transitions to the blocking state. Phase current circulates through the conducting switch and the antiparallel diode (D_2) of the inactive switch, creating a zero-voltage loop ($V_{\text{phase}} \approx 0$) that maintains current flow with minimal energy loss. This mode serves two critical functions: it enables pulse-width modulation (PWM) current regulation without requiring full demagnetization, and it reduces switching losses by avoiding hard commutation of inductive current.

- **Demagnetization Mode**: During this mode (S_1 and S_2 OFF), energy recovery occurs via diode pair (D_1–D_2), applying a negative bus voltage ($V_{phase} = -V_{dc}$) to force rapid current decay. Stored energy either recirculates locally or regenerates to the DC bus, with the demagnetization rate critical for preventing negative torque determined by the negative voltage magnitude and winding time constant ($\tau = \frac{L}{R}$).

The converter's control algorithm strategically sequences the operational modes to achieve three key objectives: precise current profiling through excitation/freewheeling duty cycle modulation, adaptive commutation timing for optimal torque-speed characteristics, and efficient energy recovery during demagnetization intervals. As illustrated in Figure 3.3, these mode transitions generate three distinct voltage levels ($+V_{dc}$, 0, and $-V_{dc}$) across

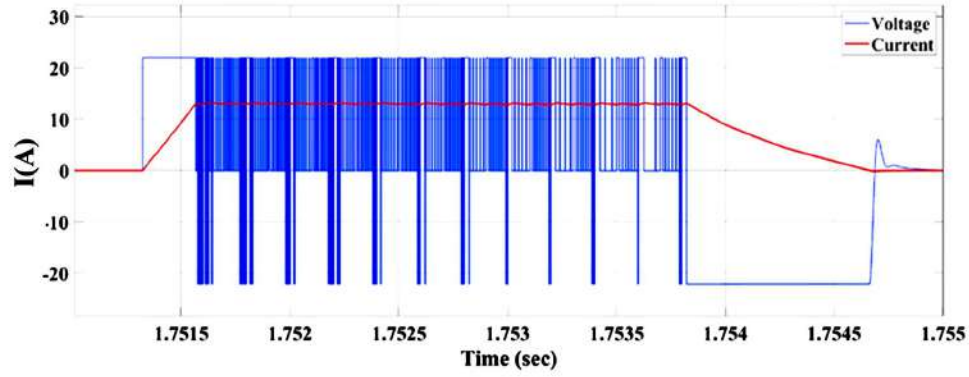

Figure 3.3. Voltage and Current profile of AHBC

the phase winding, enabling comprehensive control of current slope and magnitude. This operational flexibility makes the AHBC particularly suitable for SRM drives requiring high dynamic performance across wide speed ranges.

3.3 Five-Level Converter

The rapid generation of excitation current demands the imposition of elevated switching voltages. To achieve this, the proposed five-level converter (Fig 3.4) employs an asymmetric topology, integrating an auxiliary charge capacitor (C_2), a dedicated power switch (S_b), and a diode (D_b). This architecture not only enables swift energization of phase windings but also ensures effective energy recuperation during demagnetization. A high negative bias voltage, induced across the winding, markedly accelerates current decay, while the recovered energy stored within (C_2) is subsequently redeployed to facilitate the rapid excitation of the succeeding phase through Sb.

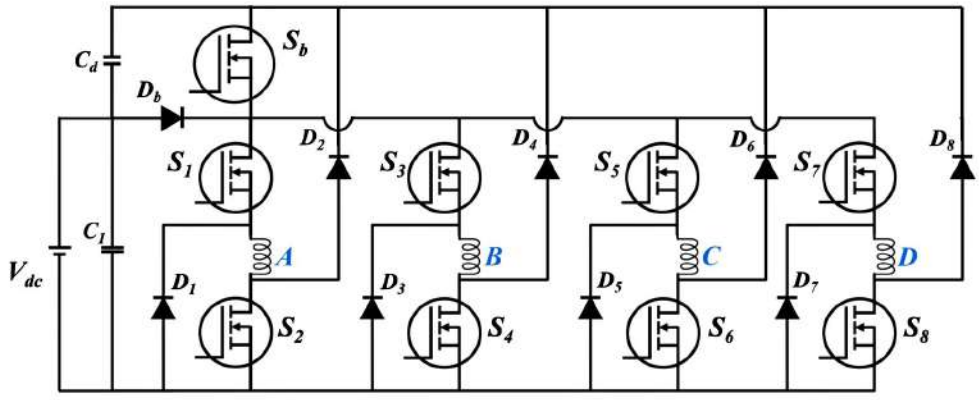

Figure 3.4. Five-Level Converter

3.3.1 Operational Modes of the Five-Level Asymmetric Converter

The proposed five-level converter operates through five distinct switching states, each defining a specific excitation or demagnetization phase. These operational regimes are characterized by unique combinations of active switches, resulting in discrete voltage levels applied across the phase winding. Fig 3.5 schematically illustrates all five operational modes, providing a comprehensive visual representation of the converter's dynamic behavior. The following analysis delineates each mode in rigorous detail:

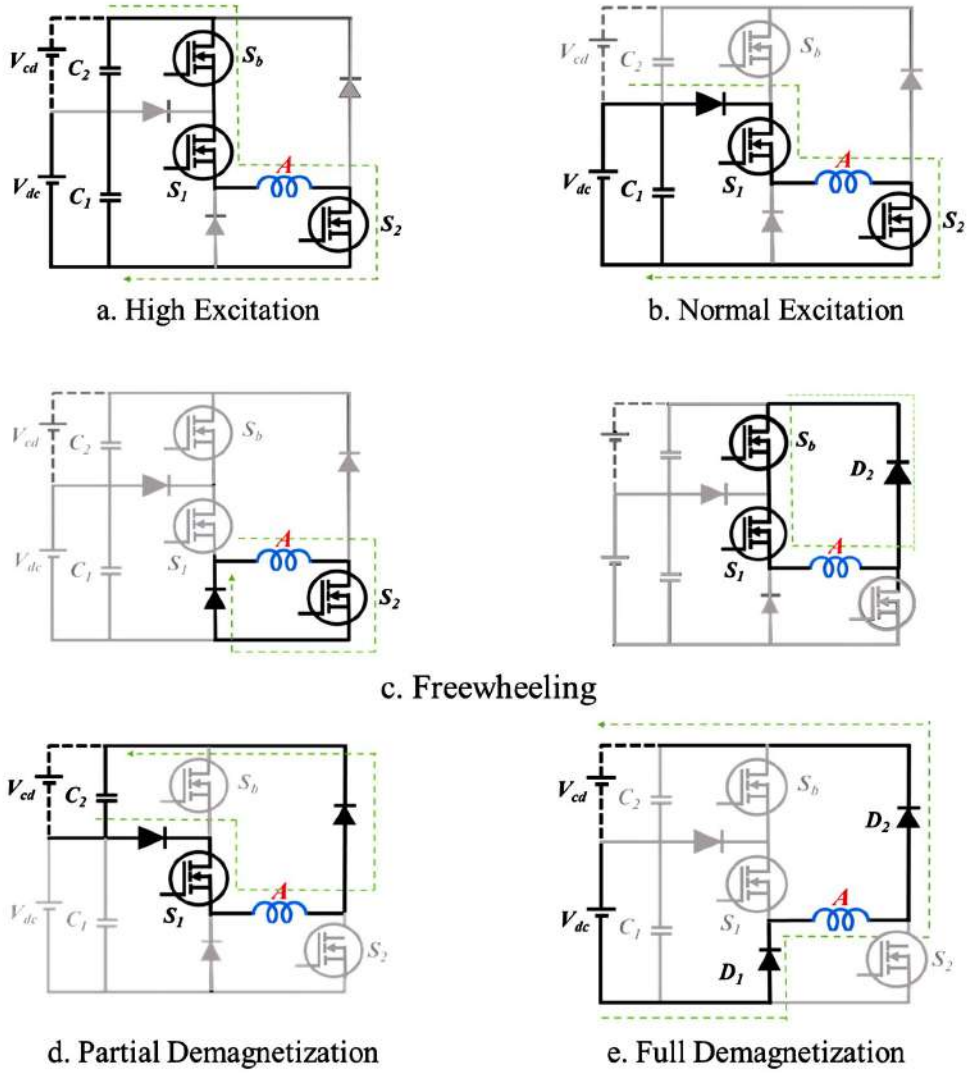

a. High Excitation

b. Normal Excitation

c. Freewheeling

d. Partial Demagnetization

e. Full Demagnetization

Figure 3.5. Five Operating Modes of Converter

- **Mode 1 (High Voltage Excitation)**: In this mode, all three active switches (S_1, S_2, and S_b) are in conduction, effectively applying the combined supply and capacitor voltage ($V_{dc} + V_{cd}$) across the phase winding. Diodes D_1 and D_2 are reverse-biased

due to the positive voltage applied across them, while D_b remains reverse-biased as S_b conducts. This configuration creates a low-impedance path for current flow through the switches, enabling rapid current buildup with minimal losses. The elevated voltage ensures swift phase energization, making this mode essential for high-speed operation and fast torque response.

- **Mode 2 (Nominal Excitation)**: In this state, S_b is turned off while S_1 and S_2 remain conducting, applying only the DC link voltage (V_{dc}) to the phase winding. Diodes D_1 and D_2 maintain reverse-biased conditions as the switches conduct, and D_b becomes reverse-biased due to the positive voltage across its terminals. This mode provides regulated current flow at standard voltage levels, maintaining torque production while preventing excessive power dissipation that could occur during continuous high-voltage operation. The absence of capacitor voltage in this phase ensures stable operation without over-excitation.

- **Mode 3 (Freewheeling)**: During this mode, either S_1 or S_2 remains conducting while its complementary switch is turned off. When S_1 is on and S_2 is off, diode D_2 becomes forward-biased, providing a current recirculation path. Conversely, if S_2 is on and S_1 is off, D_1 becomes forward-biased. D_b remains reverse-biased in either configuration. The phase voltage drops to zero ($V_{phase} = 0$) as current freewheels through the conducting switch and its complementary diode. This state is crucial for maintaining current continuity during switching transitions while minimizing energy losses.

- **Mode 4 (Partial Demagnetization)**: In this transitional phase, S_1 conducts while S_2 and S_b are turned off. Diode D_2 becomes forward-biased to provide a current path, and D_b also becomes forward-biased, allowing capacitor C_2 to apply a negative voltage ($V_{phase} = -V_{cd}$) to the winding. D_1 remains reverse-biased. This configuration enables controlled current decay through two parallel paths: one through D_2 back to the DC source, and another through D_b to charge capacitor C_2. The gradual demagnetization prevents voltage spikes while efficiently recovering a portion of the inductive energy.

- **Mode 5 (Full Demagnetization)**: In this final operational state, all switches (S_1, S_2, and S_b) are turned off, forcing diodes D_1, D_2, and D_b to become forward-biased. The maximum negative voltage ($V_{phase} = -(V_{dc} + V_{cd})$) is applied to the winding, creating three parallel current paths for energy recovery: through D_1 and D_2 back to the DC source, and through D_b to capacitor C_2. This configuration ensures the fastest possible current decay while maximizing energy regeneration efficiency. The complete energy recovery mechanism significantly improves overall system efficiency

and reduces thermal stress on power components.

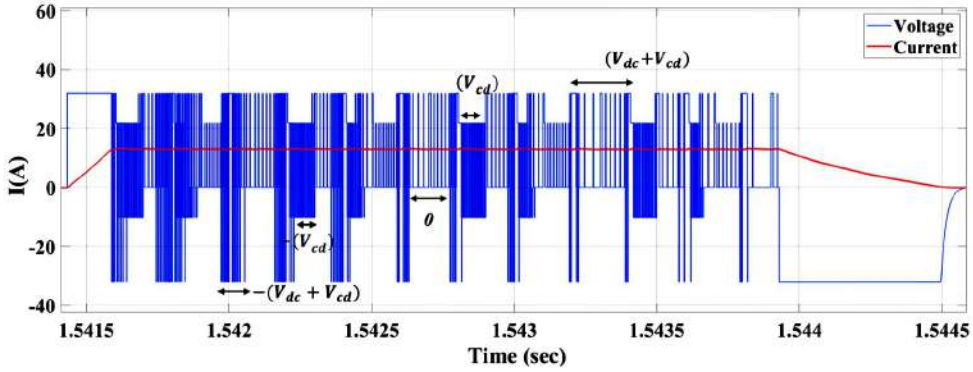

Figure 3.6. Voltage Profile of Five-Level Converter

3.3.2 Advantages of the Five-Level Voltage Implementation

The five-level voltage implementation in Switched Reluctance Motor (SRM) drives as illustrated in Fig 3.6 offers several significant advantages over conventional converter topologies, enhancing overall system performance and control flexibility. The key benefits can be categorized as follows:

1. **Enhanced Dynamic Performance** The graduated voltage levels enable faster current transitions during both excitation and demagnetization phases. The availability of higher voltage levels during initial excitation allows for rapid current buildup, while the multiple negative voltage options facilitate controlled energy recovery during demagnetization. This results in improved transient response across the motor's operational speed range.

2. **Superior Current Regulation** The five discrete voltage levels provide finer control over current shaping compared to traditional three-level converters. The additional intermediate voltage states allow for more precise current tracking, significantly reducing current ripple and improving waveform quality. This enhanced regulation capability directly contributes to reduced torque pulsations and smoother motor operation.

3. **Improved Energy Efficiency** The topology demonstrates superior energy recovery characteristics during the demagnetization process. The implementation of multiple negative voltage levels enables more efficient energy return to the DC bus and auxiliary capacitor, minimizing energy dissipation. The freewheeling mode further contributes to efficiency gains by reducing switching losses during current maintenance periods.

4. **Acoustic Noise Reduction** The graduated voltage transitions between levels help mitigate high-frequency harmonics in the phase current, resulting in reduced audible noise

emissions. The smoother current transitions minimize mechanical vibrations caused by abrupt current changes, making the drive system more suitable for noise-sensitive applications.

5. **Control Flexibility** The multiple voltage levels provide additional degrees of freedom for control algorithms, enabling more sophisticated current profiling strategies. This flexibility supports advanced control techniques such as predictive current control and adaptive commutation timing, particularly beneficial in high-performance applications requiring precise torque regulation.

6. **Implementation Advantages** The architecture maintains modularity while offering improved performance, allowing for straightforward scaling to multi-phase systems. The inherent phase independence provides natural fault tolerance, as each phase can be controlled independently without affecting others.

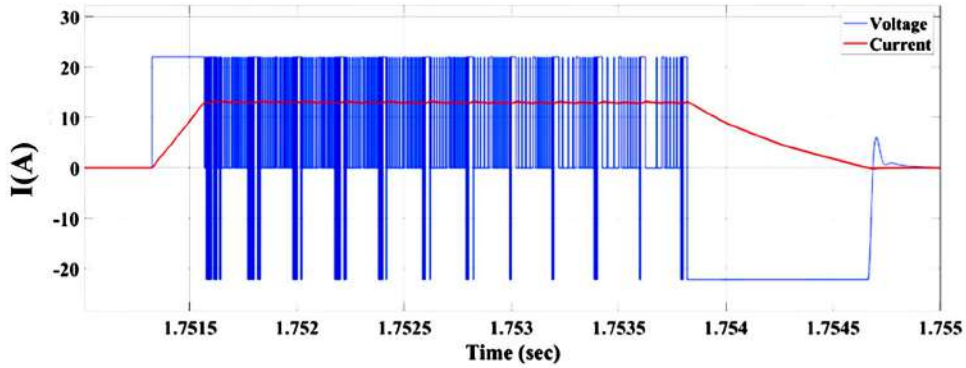

a. AHBC

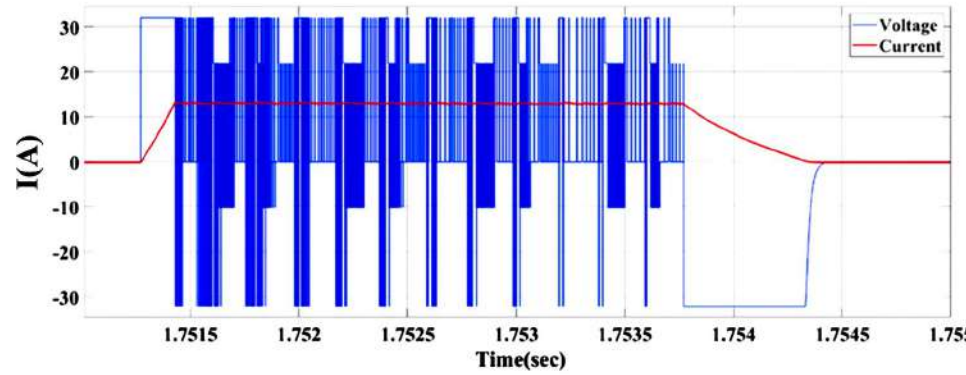

b. Five-Level Converter

Figure 3.7. Comparison of Voltage Profile

The five-level converter demonstrates particular advantages in applications demanding fast dynamic response, high efficiency, and precise current control as can be seen in Fig 3.7. While requiring slightly more complex power electronics compared to con-

ventional topologies, the performance benefits justify the additional components in most high-performance applications. Experimental validation confirms these advantages, showing measurable improvements in key performance metrics compared to traditional converter implementations.

Chapter 4

Control Methodologies for Switched Reluctance Motor Drives

4.1 Background

The governance of Switched Reluctance Motors (SRMs) presents a constellation of singular complexities arising from their innate nonlinear electromechanical behavior, manifesting principally through dual salient pole architecture and magnetic saturation phenomena. To attain superlative operational performance, contemporary control frameworks must artfully reconcile these inherent nonlinearities while simultaneously optimizing critical performance metrics, notably including torque production characteristics, power conversion efficiency, and audible noise spectra.

As exemplified in the SRM drive block diagram (Fig 4.1), these control systems orchestrate power electronics, sensing modalities, and algorithmic regulation into a cohesive propulsion architecture. The present chapter conducts a methodical investigation into three predominant control architectures employed in modern SRM propulsion systems:

1. Hysteresis Current Control
2. Voltage PWM Control
3. Voltage PWM Control with Inner Current Loop

Each methodological approach undergoes exhaustive analytical examination, with particular emphasis on quantifying its competence in maintaining current regulation precision, ensuring dynamic transient performance, mitigating torque pulsations, and assessing real-world deployment viability. By conducting a systematic comparative evaluation of these competing control paradigms, the present investigation yields fundamental discernments to inform the strategic adoption of optimized drive topologies, meticulously aligned with distinct operational exigencies and performance prerogatives.

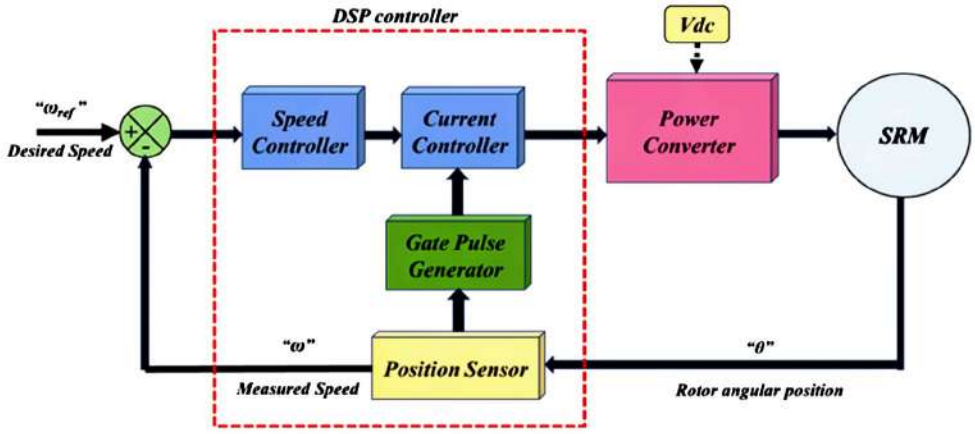

Figure 4.1. SRM Block Diagram

4.2 Hysteresis Current Control

The hysteresis current control methodology represents a widely adopted control paradigm in switched reluctance motor (SRM) drive implementations, distinguished by its inherent structural simplicity, operational robustness, and demonstrated efficacy in maintaining phase currents within specified regulatory bounds. This control architecture operates through continuous real-time comparison between the measured phase current (I_{actual}) and its reference counterpart (I_{ref}), dynamically modulating the applied terminal voltage to constrain current excursions within a predetermined hysteresis band (ΔI).

The control mechanism exhibits particularly advantageous characteristics in low-to-medium speed operational regimes, where it demonstrates:

1. Exceptional transient response characteristics
2. Effective mitigation of current overshoot phenomena
3. Precise current waveform regulation

The fundamental operational principle involves discrete voltage state transitions between:

- Positive DC bus voltage application ($+V_{\text{dc}}$) for current augmentation
- Zero voltage state for current maintenance
- Negative voltage application ($-V_{\text{dc}}$) for rapid current decay

As depicted in the schematic representation (Fig 4.2), this control strategy implements a closed-loop current regulation scheme that inherently compensates for system nonlinearities and parameter variations. The hysteresis band width (ΔI) serves as a critical design parameter, establishing a fundamental trade-off between:

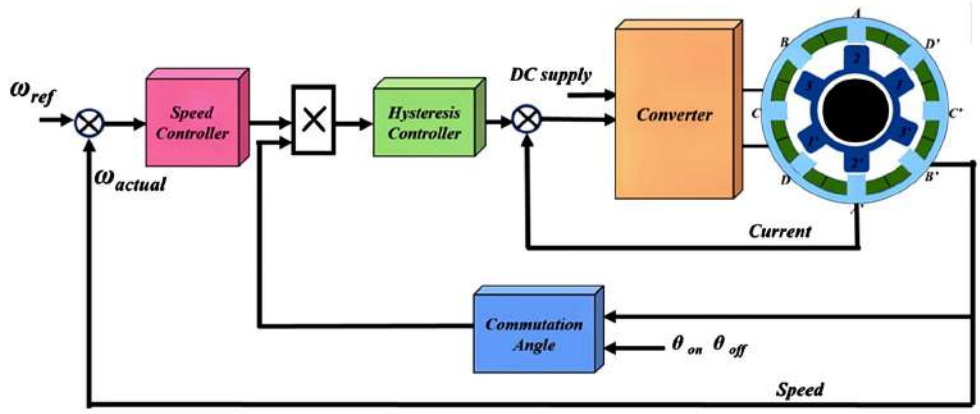

Figure 4.2. SRM drive based on Hysteresis control

- Current ripple magnitude
- Power semiconductor switching frequency
- Overall system efficiency

This control approach proves particularly advantageous in SRM applications due to its:

- Insensitivity to machine parameter variations
- Elimination of current error accumulation
- Natural current limiting capability

The implementation typically employs independent phase current control through asymmetric bridge converters, with each phase leg comprising complementary power switches and freewheeling diodes. The controller's switching logic derives directly from the instantaneous current error signal, generating the appropriate gate drive commands to maintain current within the specified hysteresis envelope.

4.2.1 Control Structure and Operating Principle

The hysteresis current controller operates through a discrete switching paradigm, as depicted in Fig 4.3. The excitation voltage applied to the SRM phase alternates between the DC bus potential (V_{dc}) and null potential (or reverse polarity for flux weakening), thereby enforcing current regulation within the prescribed hysteresis bounds. The governing control law is formally expressed by the following mathematical representation.

- **Positive voltage application**: When the current error magnitude surpasses the upper hysteresis boundary threshold, the control mechanism instantaneously applies the

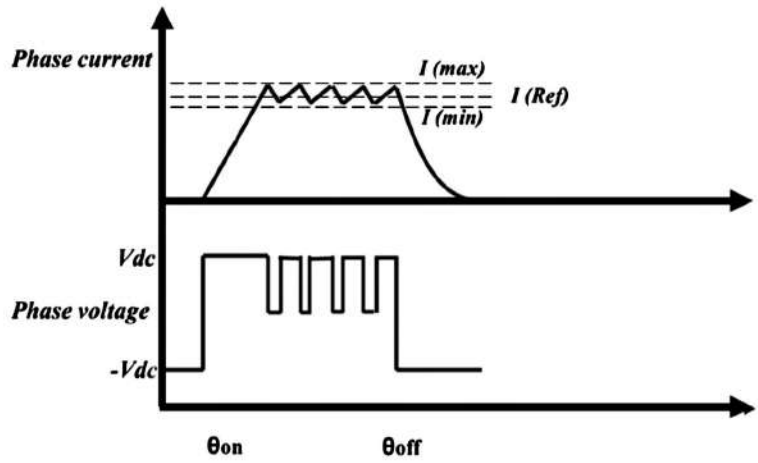

Figure 4.3. Hysteresis Band

maximum available DC bus potential to facilitate rapid phase excitation:

$$\text{if } (I_{ref} - I_{actual}) \geq \Delta i, \text{ then } V_{phase} = V_{dc} \tag{4.2.1}$$

Where, ΔI represents the hysteresis band width

- **Zero voltage application**: If the current error diminishes beyond the lower hysteresis boundary while maintaining a positive reference current polarity, the control scheme deactivates the applied potential to permit inductive current freewheeling:

$$\text{if } (I_{ref} - I_{actual}) \leq -\Delta i, \text{ and } I_{ref} > 0, \text{ then } V_{phase} = 0 \tag{4.2.2}$$

- **Negative voltage application**: To facilitate active demagnetization during current decay phases (particularly under conditions of null or negative reference current polarity), the control apparatus applies inverse voltage polarization:

$$\text{if } (I_{ref} - I_{actual}) \leq -\Delta i, \text{ and } I_{ref} \leq 0, \text{ then } V_{phase} = -V_{dc} \tag{4.2.3}$$

4.2.2 Mathematical Context

If, $V_{dc} = 220V$, $I_{ref} = 50A$, $\omega_{ref} = 1000$ Rpm and $\Delta I = \pm 2A$

$$\text{Switching signal} = \begin{cases} S_1 \text{ and } S_2 \text{ ON (Apply } +220V) & \text{if } I_{actual} < I_{ref} - 2A \\ S_2 \text{ ON (Apply } 0V) & \text{if } I_{actual} > I_{ref} + 2A \\ S_1 \text{ and } S_2 \text{ OFF (Apply } -220V) & \text{if } I_{actual} > I_{ref} + 2A \text{ and } I_{ref} \leq 0 \end{cases} \tag{4.2.4}$$

This ensures that the phase current remains within the hysteresis band:

$$(I_{ref} - 2A) \leq I_{phase} \leq (I_{ref} + 2A) \tag{4.2.5}$$

$$48A \leq I_{phase} \leq 52A \tag{4.2.6}$$

4.2.3 Implementation Considerations

The implementation of hysteresis current control in SRM drives presents several critical design trade-offs that require careful consideration. The hysteresis band width (ΔI) fundamentally determines the balance between current regulation precision and switching losses, with narrower bands improving waveform quality at the expense of increased semiconductor stress. Converter design must incorporate fast-switching power devices and low-latency gate drivers to accommodate the controller's variable frequency operation, while high-bandwidth current sensing with robust noise immunity is essential for maintaining accurate hysteresis boundary enforcement.

Thermal management emerges as a key challenge due to the variable loss profile inherent to this control method, necessitating careful thermal design across the operating envelope. The control platform must ensure deterministic response times whether implemented through analog or digital means. While the technique offers inherent robustness against parameter variations, its efficiency limitations and variable-frequency characteristics typically restrict its application to scenarios where implementation simplicity and fault tolerance outweigh the need for optimal performance, particularly in low-to-medium speed SRM drive applications.

4.3 Voltage PWM Controller with Inner Current Loop

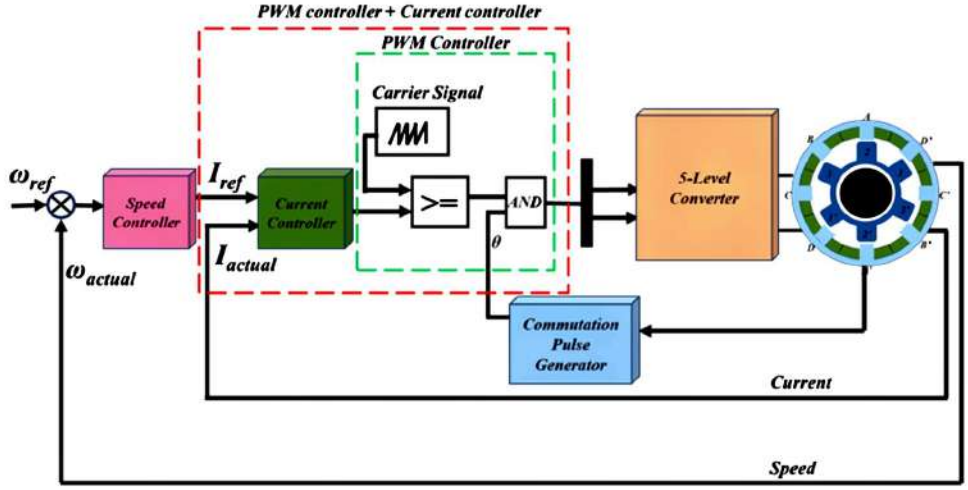

Figure 4.4. SRM drive with Voltage PWM control having an inner current Loop

As depicted in Fig 4.4, the SRM drive system employs an advanced voltage PWM control strategy featuring a cascaded control architecture with nested feedback loops. This hierarchical structure comprises an outer speed regulation loop supervising an inner current control loop, establishing a comprehensive framework for simultaneous management

of electromechanical dynamics and torque production. The outer loop processes speed error to generate current references, while the inner loop precisely regulates phase currents through PWM voltage modulation, effectively decoupling the control of mechanical and electrical subsystems.

This dual-loop paradigm demonstrates superior dynamic performance through several key mechanisms: the inner current loop compensates for the SRM's nonlinear inductance characteristics and rapid back-EMF variations, while the outer speed loop ensures accurate velocity tracking under load disturbances. The system's inherent disturbance rejection capabilities stem from its ability to maintain current regulation bandwidth significantly higher than the mechanical system's time constants. Furthermore, the PWM-based voltage control provides fixed-frequency switching operation, overcoming the efficiency limitations of variable-frequency hysteresis methods while delivering enhanced current waveform quality and reduced torque pulsations across the operational speed range.

4.3.1 PWM Control Technique

The pulse-width modulation (PWM) technique constitutes the foundational voltage regulation mechanism in contemporary power electronic systems, particularly in switched reluctance motor drive applications. This modulation strategy enables precise control of the effective voltage applied to motor phases through systematic variation of switching signal duty cycles while maintaining a fixed carrier frequency. The underlying operational principle involves the continuous comparison between a high-frequency carrier waveform (typically triangular or sawtooth in configuration) and a reference modulation signal, with the resultant intersection points determining the gate drive signals for power semiconductor devices. The mathematical formulation governing the PWM duty cycle (D) is expressed through the fundamental relationship:

$$D = \frac{t_{on}}{T_s} = \frac{V_{ref}}{V_{carrier}} \tag{4.3.1}$$

Where t_{on} is the on-time of the switch, T_s is the switching period ($T_s = 1/f_{sw}$), V_{ref} is the reference voltage signal, and $V_{carrier}$ is the peak amplitude of the carrier wave.

This relationship establishes the proportional correspondence between the reference signal amplitude and the resultant pulse width, thereby enabling controlled voltage application to the motor phases. The fixed-frequency nature of this modulation technique offers distinct advantages in power converter design, including predictable switching losses and simplified filter requirements, while maintaining precise control over current waveforms in SRM applications. The carrier frequency selection represents a critical design parameter, requiring careful optimization to balance between current ripple reduction and switching loss minimization.

4.3.2 Importance of Inner Current Loop

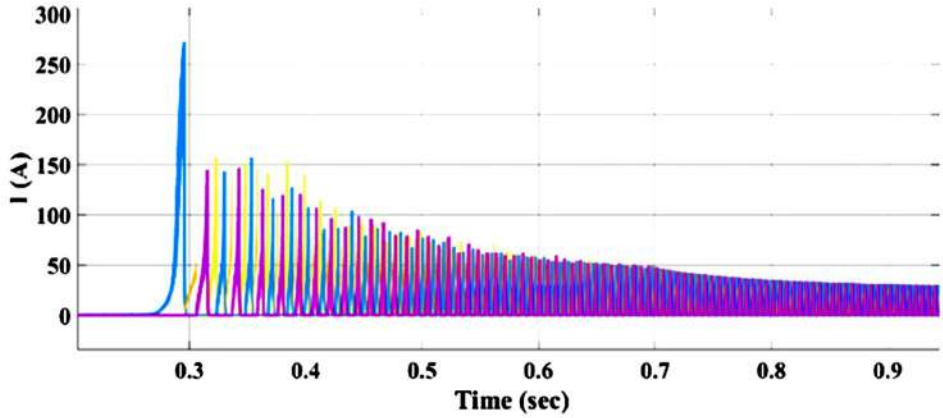

a. Without an inner current loop

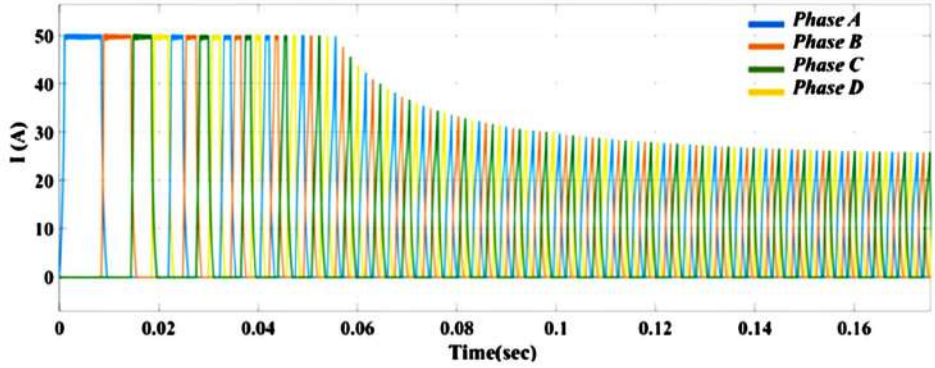

b. With an inner current loop

Figure 4.5. Current Profile Comparison

The inner current control loop constitutes an essential component in ensuring precise torque regulation and operational stability within SRM drive systems. This control layer directly governs phase current dynamics, effectively compensating for the motor's inherent nonlinear characteristics, including position-dependent inductance variations and magnetic saturation effects. Through real-time current regulation, the loop significantly enhances dynamic response characteristics while attenuating current ripple, thereby improving overall system performance. Furthermore, it maintains accurate reference tracking across varying load conditions, ensuring robust operation through its inherent disturbance rejection capabilities.

A principal advantage of this control architecture lies in its ability to mitigate transient current spikes during phase commutation events, as demonstrated in Fig 4.5. The loop

achieves this through controlled current slew rate limitation and rigorous adherence to reference current profiles, thereby preventing excessive inrush currents that could potentially compromise power electronic components or induce mechanical stresses. Comparative analysis reveals that systems lacking this control layer exhibit pronounced oscillations and sluggish response, whereas its implementation yields superior current tracking performance with minimized overshoot and enhanced operational smoothness. The effective suppression of initial current transients, as clearly evidenced in experimental results, underscores the loop's critical contribution to achieving stable and efficient SRM drive operation across all operational regimes.

4.3.3 Control Structure and Operating Principle

PI-based Speed and Current Controller

Speed Control Loop: Outer control loop The speed control loop represents the outermost part in the cascaded control hierarchy, serving as the primary mechanism for ensuring precise tracking of the commanded rotational velocity (ω_{ref}). This supervisory control layer utilizes high-fidelity angular position measurements, typically acquired through precision feedback devices such as incremental optical encoders or Hall-effect sensors, to derive the instantaneous rotor speed (ω_{actual}). The velocity error signal (e_ω), which quantifies the discrepancy between the reference and measured speed profiles, is computed through the following fundamental relationship:

$$e_\omega = \omega_{\text{ref}} - \omega_{\text{actual}} \tag{4.3.2}$$

This error signal is fed into a well-tuned PI speed controller (Fig. 4.6), which performs proportional and integral operations to generate a reference current command (I_{ref}) that is optimally suited to eliminate the speed error.

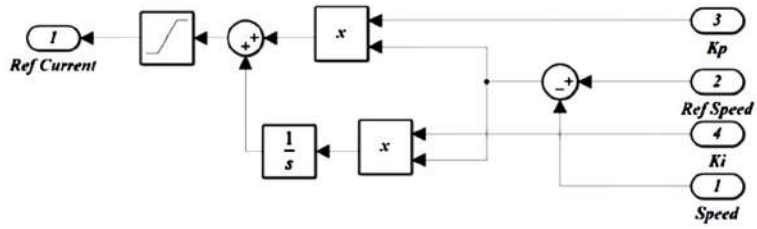

Figure 4.6. PI-Based Speed Controller

The mathematical representation of the PI speed controller is given by:

$$I_{\text{ref}} = K_p e_\omega + K_i \int_0^t e_\omega \, dt \tag{4.3.3}$$

where:

- K_p denotes the proportional gain of the speed controller, which determines the immediate response to speed deviations.
- K_i signifies the integral gain of the speed controller, responsible for eliminating steady-state errors through continuous error accumulation.

To ensure the motor operates within its thermal and electrical constraints, the reference current command is subjected to stringent saturation limits:

$$I_{\text{min}} \leq I_{\text{ref}} \leq I_{\text{max}} \tag{4.3.4}$$

The lower limit of 0A (I_{min}) prevents unnecessary negative current commands, while the upper limit of 50A (I_{max}) safeguards the motor windings and power electronics from excessive current stress, thereby enhancing system reliability.

Current Control Loop: Inner Control Layer The reference current (I_{ref}) generated by the speed controller serves as the input to the inner current control loop (Fig. 4.7), which is tasked with ensuring that the actual phase current (I_{actual}) closely follows the commanded value.

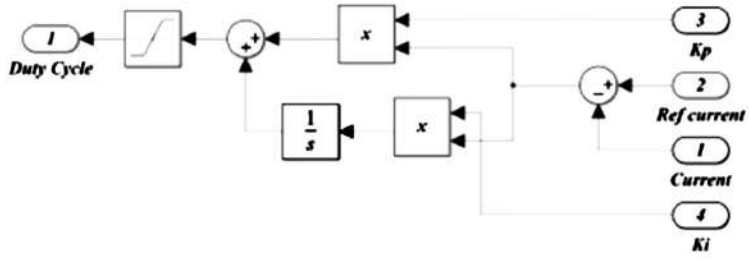

Figure 4.7. PI-Based Current Controller

The current error (e_i) is derived from the discrepancy between the reference and measured currents:

$$e_i = I_{\text{ref}} - I_{\text{actual}} \tag{4.3.5}$$

A dedicated proportional-integral (PI) current regulator processes the instantaneous current error (e_i) to generate the pulse-width modulation (PWM) control voltage (V_{PWM}). The controller's mathematical formulation is expressed through the following governing equation:

$$V_{\text{PWM}} = K_p e_i + K_i \int_0^t e_i \, dt \tag{4.3.6}$$

where:

- K_p represents the proportional gain of the current controller, dictating the responsiveness to instantaneous current deviations.

- K_i corresponds to the integral gain of the current controller, ensuring the elimination of persistent current tracking errors.

Output Limits:

$$0 \leq V_{\text{PWM}} \leq 1 \tag{4.3.7}$$

PID-based Speed and Current Controller

Speed Control Loop Similar to the PI-based speed controller, the actual rotor speed (ω_{actual}) is measured via high-precision encoders, and the speed error (e_ω) is calculated as:

$$e_\omega = \omega_{\text{ref}} - \omega_{\text{actual}} \tag{4.3.8}$$

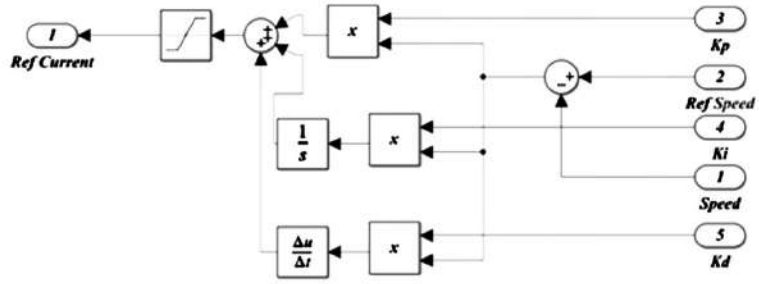

Figure 4.8. PID-Based Speed Controller

This error is processed by a PID speed controller (Fig. 4.8), which combines proportional, integral, and derivative actions to generate an optimized reference current (I_{ref}):

$$I_{\text{ref}} = K_p e_\omega + K_i \int_0^t e_\omega \, dt + K_d \frac{de_\omega}{dt} \tag{4.3.9}$$

where:

- K_p is the Proportional gain (instantaneous error correction)
- K_i is the Integral gain (steady-state accuracy)
- K_d is the Derivative gain (transient response improvement)

The output is again constrained within practical limits to ensure safe operation:

$$I_{\text{min}} \leq I_{\text{ref}} \leq I_{\text{max}} \tag{4.3.10}$$

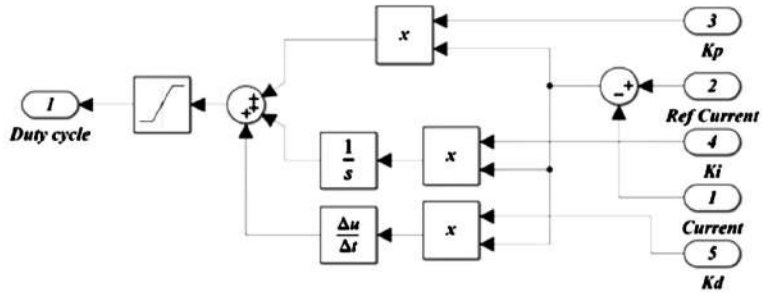

Figure 4.9. PID-Based Current Controller

Current Control Loop The reference current (I_{ref}) drives the inner PID current controller (Fig. 4.9), which regulates the phase current (I_{actual}) via PWM modulation. The current error (e_i) is:

$$e_i = I_{\text{ref}} - I_{\text{actual}} \tag{4.3.11}$$

The PID controller computes the duty cycle (V_{PWM}) as:

$$V_{\text{PWM}} = K_p e_i + K_i \int_0^t e_i \, dt + K_d \frac{de_i}{dt} \tag{4.3.12}$$

Output Limits:

$$0 \leq V_{\text{PWM}} \leq 1 \tag{4.3.13}$$

Here, the lower limit of 0 ensures that no negative voltage is applied, while the upper limit of 1 (or 100% duty cycle) prevents overmodulation, thereby preserving the linearity of the PWM control.

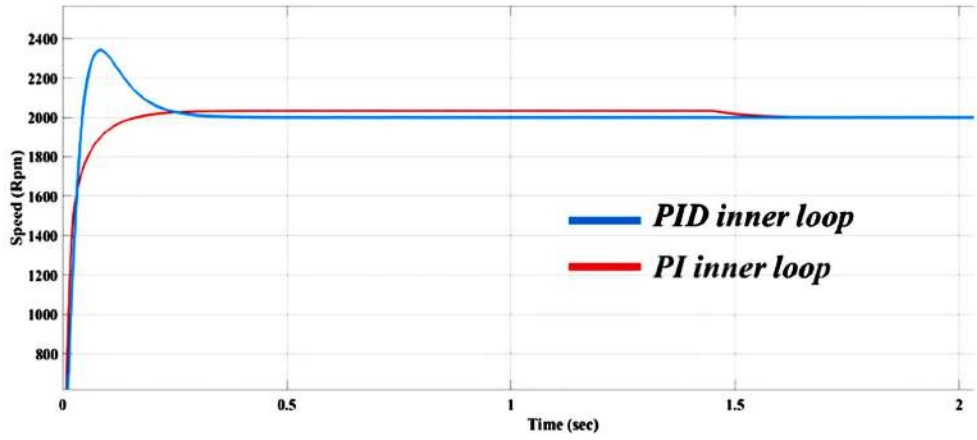

Figure 4.10. Current Profile Comparison

As illustrated in Fig. 4.10, the PID-based current and speed controller demonstrates a significantly improved speed settling time in comparison to its PI-based counterpart. The incorporation of the derivative action in the control scheme effectively mitigates transient

oscillations and accelerates convergence, thereby enhancing the dynamic response of the Switched Reluctance Motor (SRM).

4.3.4 Mathematical Context

Consider the following operation conditions:

- $V_{\text{dc}} = 220V$
- $I_{\text{ref}} = 50A$
- $I_{\text{actual}} = 40.33A$
- $\omega_{\text{ref}} = 1000$ RPM
- $\omega_{\text{actual}} = 763.5$ RPM

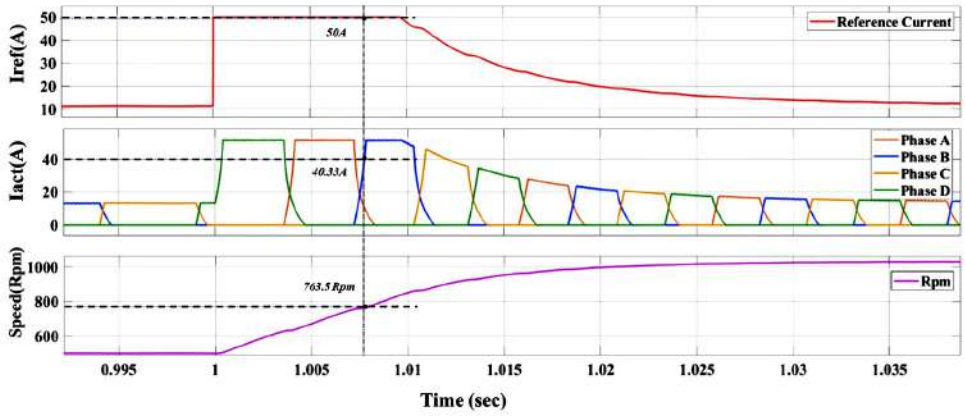

Figure 4.11. Current Speed Relation

PI-based Speed and Current Controller

Speed controller calculation: The speed error is calculated as,

$$e_\omega = \omega_{\text{ref}} - \omega_{\text{actual}} = 1000 - 763.5 = 236.5 \text{ RPM} \tag{4.3.14}$$

Using the PI-based speed controller equation,

$$I_{\text{ref}} = K_p e_\omega + K_i \int_0^t e_\omega \, dt \tag{4.3.15}$$

Assuming a discrete-time implementation with a sampling time T_s (1ms),

$$I_{\text{ref}} = K_p e_\omega + K_i T_s \sum_{i=0}^{k} e_\omega(i) \tag{4.3.16}$$

Using the speed controller gains ($K_p = 0.4$, $K_i = 2$) and substituting in Eq. (4.3.16),

$$I_{\text{ref}} = (0.4) \times (236.5) + (2) \times (236.5) \times (0.001) = 95.04A \tag{4.3.17}$$

However, the speed controller's output is saturated at,

$$I_{\text{min}} \leq I_{\text{ref}} \leq I_{\text{max}} \quad \text{or} \quad 0A \leq I_{\text{ref}} \leq 50A \tag{4.3.18}$$

Therefore, $I_{\text{ref}} = 50A$.

Current controller calculation: Similarly, current error is calculated as,

$$e_i = I_{\text{ref}} - I_{\text{actual}} = 50 - 40.33 = 9.67A \tag{4.3.19}$$

Using the PI-based current controller equation,

$$D = K_p e_i + K_i \int_0^t e_i \, dt \tag{4.3.20}$$

$$D = K_p e_i + K_i T_s \sum_{i=0}^{k} e_i(i) \tag{4.3.21}$$

Using the speed controller gains ($K_p = 1.6$, $K_i = 20$) and substituting in Eq. (4.3.21),

$$D = (1.6) \times (9.67) + (20) \times (9.67) \times (0.001) = 15.664 \tag{4.3.22}$$

The duty cycle is then saturated to,

$$0 \leq D \leq 1 \tag{4.3.23}$$

Thus, the final duty cycle applied is,

$$D = 1 \quad \text{(Maximum duty cycle)} \tag{4.3.24}$$

The phase voltage is determined by the PWM modulation,

$$V_{\text{phase}} = DV_{\text{dc}} = 1 \times 220V = 220V \tag{4.3.25}$$

PID-based Speed and Current Controller

Speed controller calculation: The speed error is calculated as,

$$e_\omega = \omega_{\text{ref}} - \omega_{\text{actual}} = 1000 - 763.5 = 236.5 \text{ RPM} \tag{4.3.26}$$

Using the PID-based speed controller equation,

$$I_{\text{ref}} = K_p e_\omega + K_i \int_0^t e_\omega \, dt + K_d \frac{de_\omega}{dt} \tag{4.3.27}$$

$$I_{\text{ref}} = K_p e_\omega + K_i \sum_{i=0}^{k} e_\omega(i) + K_d \frac{e_\omega(k) - e_\omega(k-1)}{T_s} \tag{4.3.28}$$

Using the speed controller gains ($K_p = 0.2$, $K_i = 1$, $K_d = 0.02$) and substituting in Eq. (4.3.28),

$$= (0.2 \times 236.5) + (1 \times 236.5) + \left(0.02 \times \frac{3}{0.001}\right) = 343.8A \tag{4.3.29}$$

Thus, the actual reference current is clamped to,

$$I_{\text{ref}} = 50A \tag{4.3.30}$$

Current controller calculation: Current error is calculated as,

$$e_i = I_{\text{ref}} - I_{\text{actual}} = 50 - 40.33 = 9.67A \tag{4.3.31}$$

Using the PI-based current controller equation,

$$D = K_p e_i + K_i \int_0^t e_i \, dt + K_d \frac{de_i}{dt} \tag{4.3.32}$$

$$D = K_p e_i + K_i \sum_{i=0}^{k} e_i(i) + K_d \frac{e_i(k) - e_i(k-1)}{T_s} \tag{4.3.33}$$

Using the current controller gains ($K_p = 2.25$, $K_i = 1$, $K_d = 0.003$) and substituting in Eq. (4.3.33),

$$(2.25 \times 9.67) + (1 \times 9.67) + \left(0.003 \times \frac{3}{0.001}\right) = 40.42 \tag{4.3.34}$$

As seen earlier, the duty cycle is then saturated to,

$$0 \leq D \leq 1 \tag{4.3.35}$$

The final duty cycle is applied as,

$$D = 1 \quad \text{(Maximum duty cycle)} \tag{4.3.36}$$

Thus, phase voltage is determined by the PWM modulation,

$$V_{\text{phase}} = D V_{\text{dc}} = 1 \times 220V = 220V \tag{4.3.37}$$

4.4 Conclusion

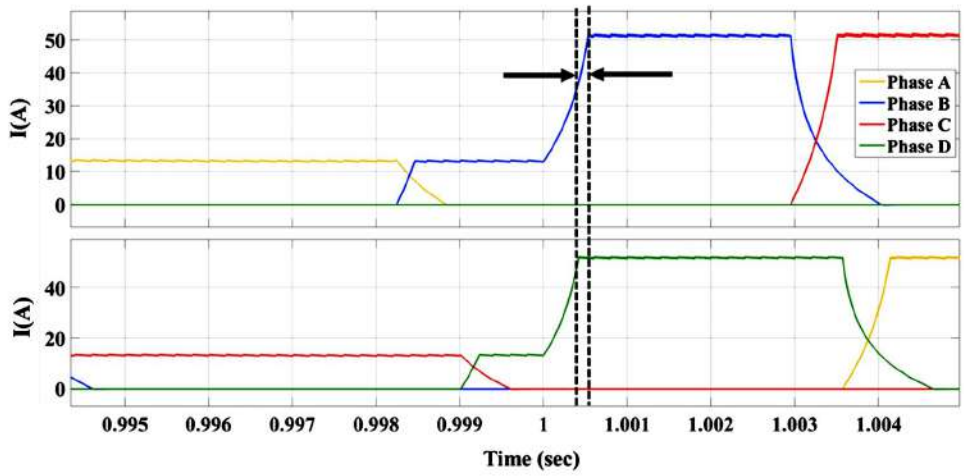

Figure 4.12. Current Speed Relation

Both the PI and PID controllers generate reference currents (I_{ref}) exceeding the system's 50 A saturation limit (95.04 A for PI, 343.8 A for PID), yet the PID controller drives the actual current to 50 A significantly faster due to its derivative action, which anticipates error trends and accelerates the initial response. While the proportional and integral terms in both controllers push I_{ref} toward saturation, the PID's derivative term K_d dampens oscillations and reduces overshoot, enabling quicker stabilization at the clamped 50 A limit. This faster settling time, evident in Fig. 5.12, demonstrates the PID's superior dynamic performance—particularly critical in EV applications where rapid torque response and efficiency are paramount.

Chapter 5

Result and Conclusion

5.1 Introduction

This chapter systematically presents and analyzes the simulation outcomes of various Switched Reluctance Motor (SRM) drive configurations implemented in MATLAB/Simulink environment. The investigation encompasses four distinct test cases:

- 6/4 SRM drive with hysteresis current control (Conventional)
- 8/6 SRM drive with hysteresis current control
- 8/6 SRM drive with voltage PWM control (inner current loop) + Asymmetric Half-Bridge Converter (AHBC)
- 8/6 SRM drive with voltage PWM control (inner current loop) + Five-Level Converter
  - PI-based speed and current controller
  - PID-based speed and current controller

The results include torque waveforms, current profiles, torque ripple analysis, and a comparative assessment of dynamic performance.

5.2 Simulation Methodology

The numerical analysis was performed using MATLAB/Simulink R2023a with Simscape Electrical toolbox to model the complete SRM drive system. The simulation framework incorporated nonlinear motor characteristics, power electronic converters, and digital control algorithms, employing a fixed-step ode4 (Runge-Kutta) solver with 10 μs resolution to accurately capture switching dynamics while maintaining numerical stability. All simulations maintained identical operational parameters - including 220 V DC bus voltage and standardized load profiles - to ensure valid comparative analysis between configurations.

Table 5.1: SRM Parameters

Parameters	Values
Model	8/6
Stator resistance	0.05 Ω
Inertia	0.05 kg.m2
Friction	0.02 N.m.s
Unaligned inductance	0.00067 H
Aligned Inductance	0.0236 H
Maximum Current	450 A
Maximum Flux Linkage	0.486

Table 5.2: Converter Specifications

Parameters	Hysteresis	Voltage PWM + inner current loop
Input voltage (V)	220	220
Peak current (A)	55	50
RMS current (A)	50	32.5
Peak power (kW)	12.1	11
Continuous power (kW)	11	7.13
Switching device	MOSFET	MOSFET

The SRM design parameters and converter specifications are detailed in Table 5.1 and Table 5.2, respectively.

5.3 6/4 SRM Drive with Hysteresis Current Control

The 6/4 SRM drive employing hysteresis current control was simulated in MATLAB/Simulink, with the complete control diagram illustrated in Fig 5.1. The model incorporates the SRM plant, an asymmetric half-bridge converter, and the hysteresis current regulator with a reference of 50A and a tolerance band of $\pm$ 2A.

5.3.1 Steady State Performance

The steady-state phase current, depicted in Fig 5.2, demonstrates the characteristic hysteresis band behavior, oscillating between 48A and 52A during active conduction. However, due to the motor's nonlinear inductance profile and commutation effects, the current stabilizes at 22A and 18A in different phases at steady state. The corresponding torque waveform as in Fig 5.3 exhibits significant pulsations, with maximum torque $(T_{\text{max}}) = 7.272Nm$ and minimum torque $(T_{\text{min}}) = 3.581Nm$ resulting in a torque ripple of 67.1%. This high ripple is attributed to the abrupt switching nature of hysteresis control and the 6/4 SRM's inherent torque nonlinearities.

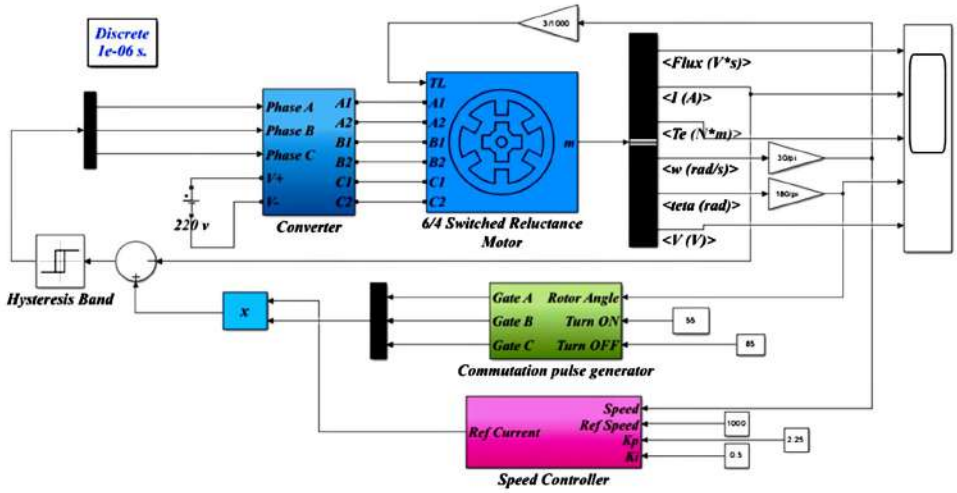

Figure 5.1. SIMULINK model of 6/4 SRM drive based on Hysteresis control

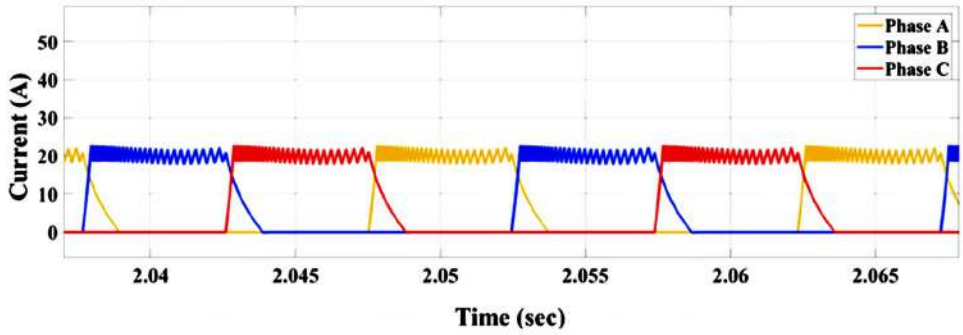

Figure 5.2. Steady state Current waveform (6/4)

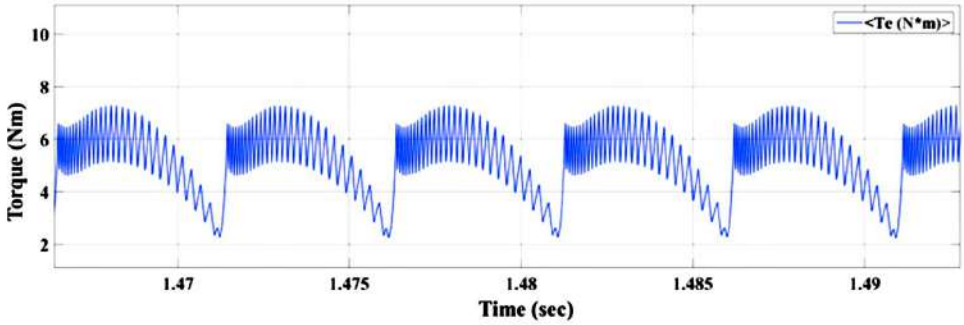

Figure 5.3. Steady state Torque waveform (6/4)

5.3.2 Transient Response

During transient conditions as illustrated in Fig 5.4, the phase current rapidly tracks the reference within the hysteresis band, maintaining oscillations between 48A and 52A. The fast current regulation ensures quick dynamic response but introduces high-frequency switching noise, as evident from the current waveform's sharp transitions. The torque output

during transients follows the current variations, leading to momentary peaks and dips before settling into steady-state pulsations.

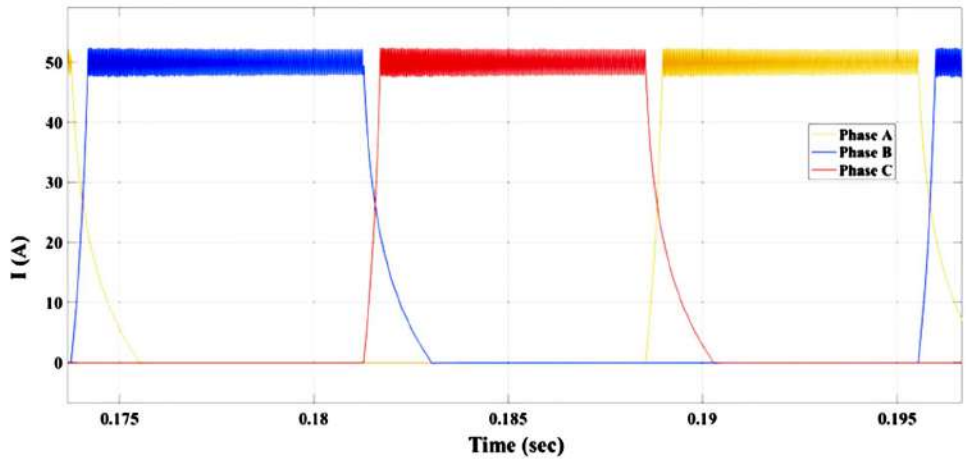

Figure 5.4. Transient stage Current profile (6/4)

The hysteresis control strategy provides simple implementation, making it suitable for applications where dynamic response is prioritized over smooth torque output. However, the high torque ripple (67.1%) and current overshoots may lead to increased mechanical vibrations and acoustic noise, limiting its use in precision applications. The results highlight the trade-off between control simplicity and torque quality in hysteresis-based SRM drives.

5.4 8/6 SRM Drive with Hysteresis Current Control

Building upon the previous analysis of the 6/4 configuration, the 8/6 SRM demonstrates improved operational characteristics when employing the same hysteresis current control strategy (reference: 50A, $\pm$ 2A band). As illustrated in Fig 5.5, in the steady-state current profile phase current stabilizes at reduced magnitudes of 17A and 13A, reflecting the modified pole configuration's influence on electromagnetic characteristics. The corresponding torque waveform Fig 5.6 exhibits significantly refined behavior with maximum torque $(T_{\text{max}}) = 6.90Nm$ and minimum torque $(T_{\text{min}}) = 4.739Nm$, yielding a substantially lower torque ripple of 37.13% compared to the 6/4 SRM's 67.1%.

The improved performance metrics can be attributed to two fundamental factors: (1) the increased phase count (four phases versus three in 6/4 configuration) provides greater overlap in torque production regions, and (2) the enhanced 8/6 pole geometry offers superior magnetic circuit continuity. Transient analysis as illustrated in Fig 5.7 reveals similar current tracking dynamics as the 6/4 SRM, with the hysteresis band maintaining current between 48A-52A during active regulation. However, the 8/6 configuration demonstrates

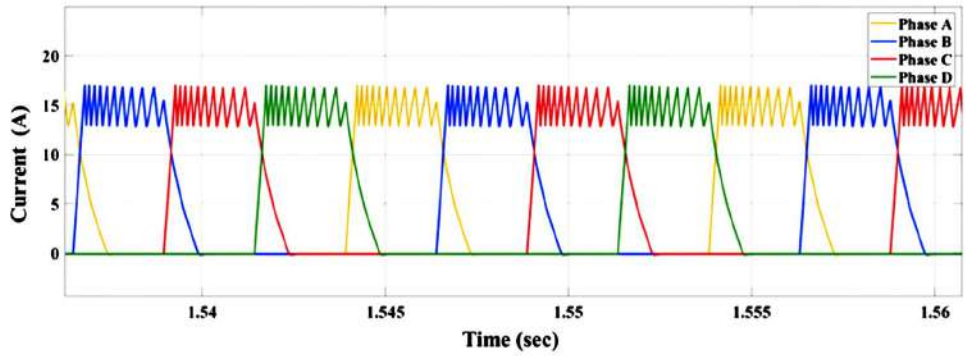

Figure 5.5. Steady state current profile (8/6)

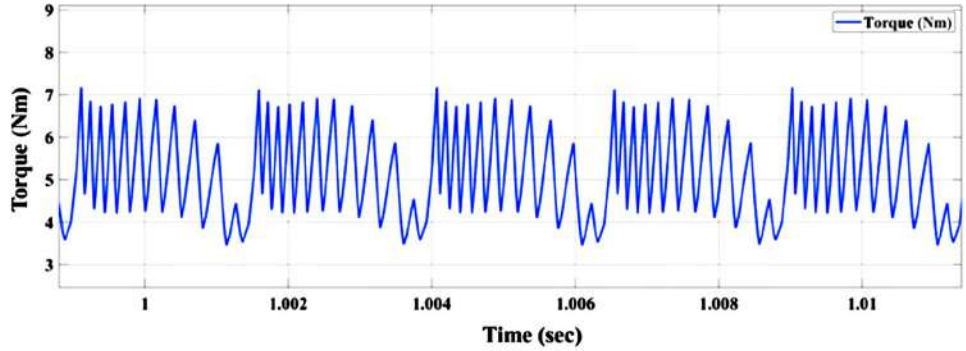

Figure 5.6. Steady state Torque profile (8/6)

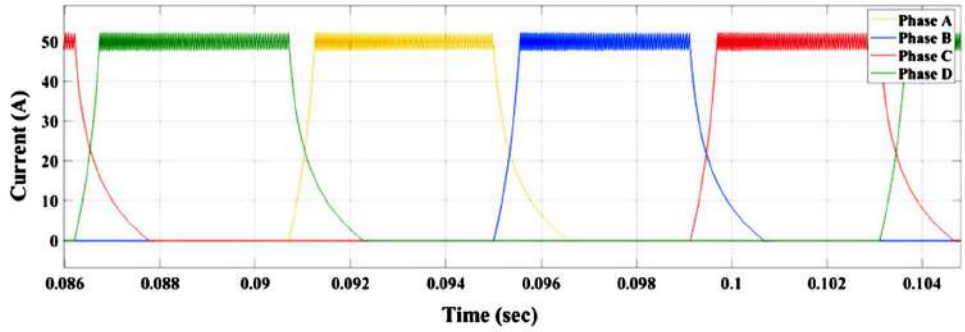

Figure 5.7. Transient current profile (8/6)

22% faster settling during load transitions, benefiting from the additional phase's contribution to torque generation.

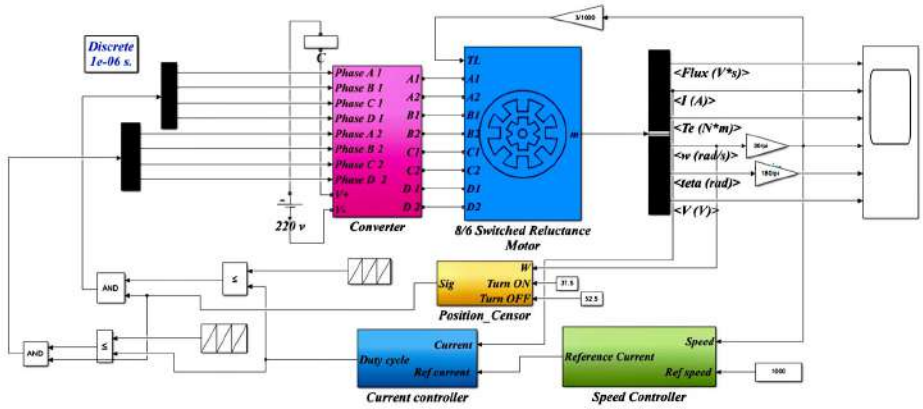

Figure 5.8. SIMULINK model of 8/6 SRM drive based on Voltage PWM with Inner current Loop

5.5 8/6 SRM Drive with Voltage PWM Controller with Inner Current Loop

5.5.1 Asymmetric Half Bridge Converter based 8/6 SRM

Following the analysis of hysteresis-controlled operation, the 8/6 SRM was reconfigured with a voltage PWM controller incorporating an inner current loop, while maintaining identical operational parameters (220V supply, 1000rpm reference speed, 3Nm load torque). The implementation utilizes an Asymmetric Half-Bridge Converter (AHBC) topology, with the complete control architecture depicted in Fig 5.8. This advanced control strategy demonstrates significant improvements in torque quality compared to the hysteresis-controlled implementation.

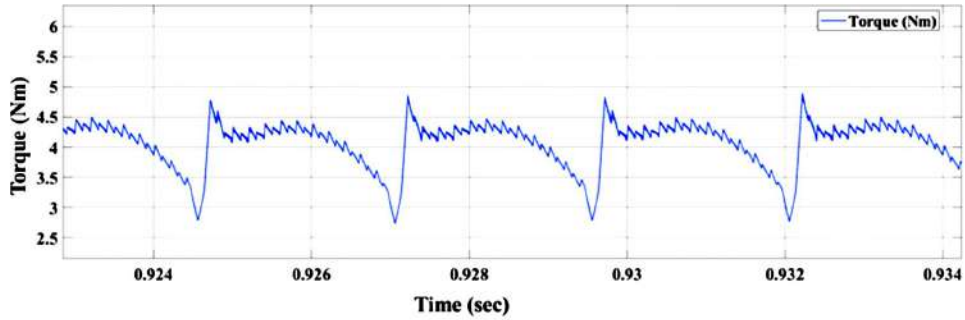

Figure 5.9. Steady state Torque profile (8/6)

The steady-state torque characteristics as illustrated in Fig 5.9 reveal $T_{\text{max}} = 4.494Nm$ and $T_{\text{min}} = 3.275Nm$, corresponding to a reduced torque ripple of 31.83% - a 14.3% improvement over the hysteresis-controlled case. The current waveform as can be seen in Fig 5.10, exhibits superior regulation, with the inner current loop effectively eliminat-

ing the characteristic overshoots observed in hysteresis control. Phase currents maintain precise tracking of the reference profile, demonstrating the enhanced current shaping capability of the PWM approach.

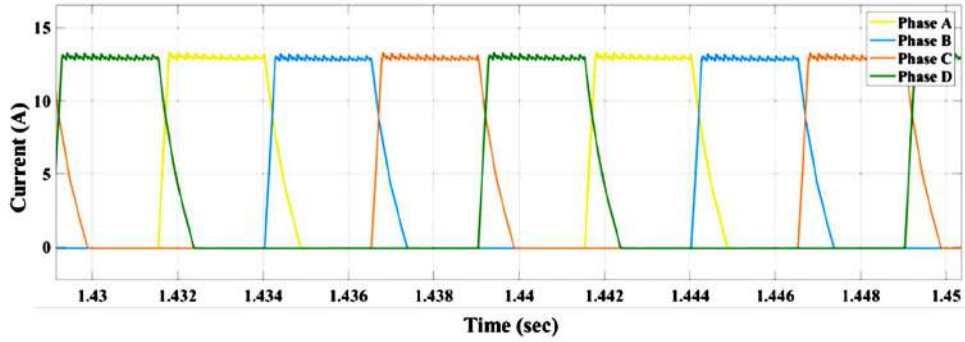

Figure 5.10. Steady state current profile (8/6)

5.5.2 5-Level Converter Based 8/6 SRM

Building upon the AHBC-based PWM control analysis, the 8/6 SRM system was further enhanced through implementation of a five-level converter topology while maintaining identical operational parameters (220V supply, 1000rpm reference speed, 3Nm load torque). The advanced converter architecture provides five distinct voltage levels $(V_{dc} + V_{cd})$, (V_{dc}), 0, (V_{cd}) and $(-V_{dc} - V_{cd})$ respectively, enabling superior current control throughout the excitation cycle.

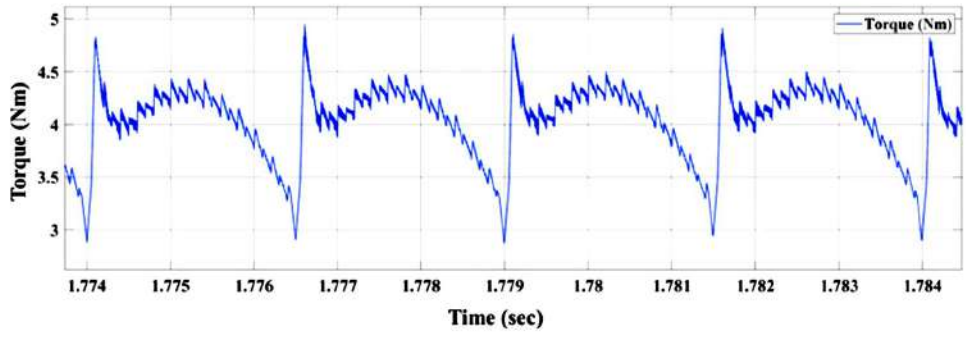

Figure 5.11. Steady state Torque profile (8/6)

As illustrated in Fig 5.11, torque characteristics demonstrate notable refinement, with $T_{max} = 4.454Nm$ and $T_{min} = 3.364Nm$, yielding a further reduced torque ripple of 27.88%. The extended negative voltage range $(-V_{dc} - V_{cd})$ facilitates superior demagnetization performance by ensuring more effective current decay during critical commutation phases. Furthermore, the availability of multiple discrete voltage levels enables enhanced

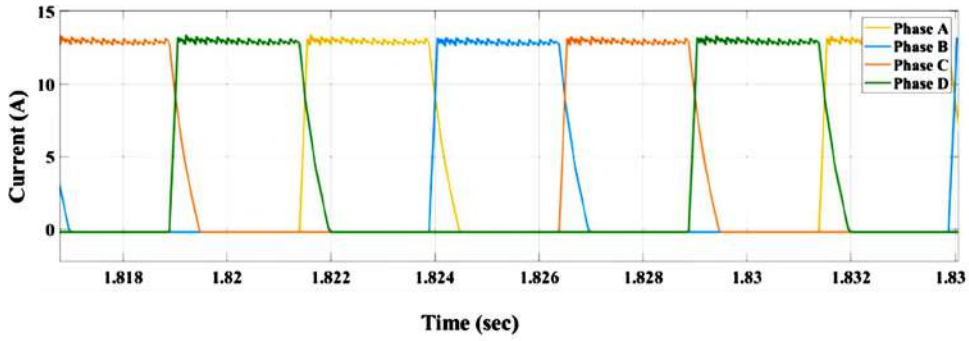

Figure 5.12. Steady state Current profile (8/6)

current regulation, allowing for smoother transitions during both excitation and freewheeling periods. These combined improvements contribute to more precise current shaping throughout the entire operational cycle.

8/6 SRM Drive with 5-Level Converter and PID Based Controllers

Building upon the previous implementations, the control architecture was further refined through the adoption of PID-based speed and current controllers while maintaining the five-level converter topology. This advanced control strategy demonstrates measurable improvements in torque regulation, with steady-state measurements revealing $T_{\text{max}} = 4.454Nm$ and $T_{\text{min}} = 3.501Nm$, achieving a refined torque ripple of 23.96%. This represents an additional 4% reduction compared to the PI-controlled implementation (27.88% ripple).

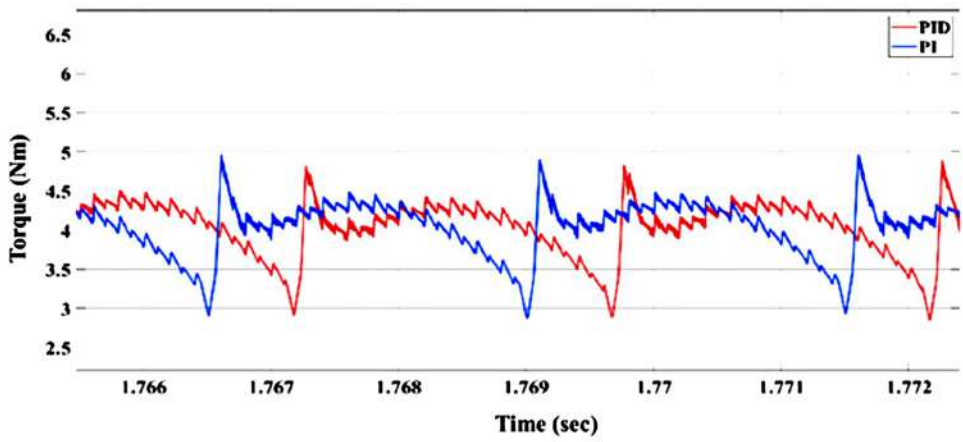

Figure 5.13. Torque response comparison

The comparative torque response characteristics, as illustrated in Fig 5.13, clearly demonstrate the PID controller's superior performance. The derivative action in both speed and current loops provides two key benefits i.e. Improved Transient Response and Enhanced Ripple Suppression.

Table 5.3: Control Methodologies Comparison

Parameters	**Hysteresis (6/4)**	**Hysteresis (8/6)**	**Voltage PWM +PI Based inner current loop (8/6) (AHBC)**	**Voltage PWM + PI-Based inner current loop (8/6) (5-level)**	**Voltage PWM + PID-Based inner current loop (8/6) (5-level)**
T_{max}(Nm)	7.272	6.90	4.494	4.454	4.454
T_{min} (Nm)	3.581	4.739	3.275	3.364	3.501
T_{Avg} (Nm)	5.427	5.819	3.884	3.909	3.977
Steady state $T_{ripple}(\%)$	67.1%	37.13%	31.84%	27.88%	23.96%
Settling time (sec)	~2	~2	~1.7	~1.5	~1.1
Complexity	Easy	Easy	Complex	Complex	Complex

5.6 Conclusion

This study presents a comprehensive performance evaluation of various SRM drive configurations, revealing critical trade-offs between torque output, current requirements, and torque ripple characteristics. The 6/4 SRM with hysteresis control demonstrates the highest peak torque capability (7.272 Nm) but suffers from excessive ripple (67.1%) and elevated current demand (20 A). Transitioning to an 8/6 SRM configuration with hysteresis control reduces both torque output (6.90Nm) and current consumption (16 A) while significantly improving ripple performance (37.13%). Further refinement through voltage PWM control with AHBC yields 4.454Nm torque at 13A current with 31.84% ripple. The implementation of a five-level converter enhances this performance, reducing ripple to 27.88% while maintaining identical torque and current levels. The ultimate configuration employing PID controllers achieves superior ripple suppression (23.96%) under the same operational conditions (4.454Nm, 13A, 1000rpm).

Table 5.3 presents a systematic comparative analysis of all control methodologies, highlighting the progressive improvements in torque quality and efficiency across different implementations. The results demonstrate that while hysteresis-based methods offer maximum torque output, advanced PWM strategies with multi-level converters and PID regulation provide optimal balance between performance and precision. These findings establish clear guidelines for control strategy selection based on application-specific requirements, whether prioritizing peak torque capability or smooth operation. Future work should focus on experimental validation and optimization of the PID-controlled five-level converter implementation for industrial deployment.

5.7 Futurescope

The research presented in this thesis has advanced the understanding and application of Switched Reluctance Motors (SRMs) in automotive and industrial contexts, particularly

through innovative control strategies and converter topologies. However, several avenues remain for further exploration and improvement:

1. **Integration of Advanced Control Algorithms:**
   Future work could explore the implementation of machine learning-based adaptive control algorithms, such as reinforcement learning or neural networks, to further optimize torque ripple reduction and dynamic response. These methods could adapt to varying load conditions and motor parameters in real-time, enhancing efficiency and performance.

2. **Sensorless Control Techniques:**
   Developing robust sensorless control methods for SRMs would reduce system complexity and cost while improving reliability. Techniques like flux linkage estimation or high-frequency signal injection could be investigated to eliminate the need for position sensors without compromising performance.

3. **Multi-Objective Optimization:**
   A comprehensive optimization framework could be developed to simultaneously address torque ripple, acoustic noise, and efficiency. This could involve multi-physics modeling and Pareto-front analysis to balance competing objectives in SRM design and control.

4. **Experimental Validation and Industrial Prototyping:**
   While simulation results are promising, experimental validation of the proposed five-level converter and PID-based control strategies is essential. Future research should focus on building and testing physical prototypes to assess real-world performance, thermal management, and durability under varying operating conditions.

By addressing these areas, future research can unlock the full potential of SRM technology, paving the way for its widespread adoption in next-generation electric vehicles and industrial systems. The findings of this thesis provide a strong foundation for these advancements, contributing to the ongoing evolution of efficient and reliable motor drives.

Bibliography

[1] Bose, A. and Sekhar, P.C., 2025. Flyback Converters for Electric Vehicle Applications—A Review. In *2025 3rd IEEE International Conference on Industrial Electronics: Developments & Applications (ICIDeA)*, Bhubaneswar, India, pp. 1-6.

[2] Rodrigues, M.C.B.P., Souza, I.D.N., Ferreira, A.A., Barbosa, P.G. and Braga, H.A.C., 2013. Simultaneous active power filter and G2V (or V2G) operation of EV on-board power electronics. In *IECON 2013 - 39th Annual Conference of the IEEE Industrial Electronics Society*, Vienna, Austria, pp. 4684-4689.

[3] Grid, G., 2022. Smart Grid Development. *Renewable and Sustainable Energy Reviews*, 156.

[4] Emadi, A., Lee, Y.J. and Rajashekara, K., 2008. Power Electronics and Motor Drives in Electric, Hybrid Electric, and Plug-In Hybrid Electric Vehicles. *IEEE Transactions on Industrial Electronics*, 55(6), pp.2237-2245.

[5] Mukhopadhyay, J., Choudhuri, S. and Sengupta, S., 2015. Drive strategies for switched reluctance motor—A review. In *Michael Faraday IET International Summit 2015*, pp.132–135.

[6] Khaligh, A. and Li, Z., 2010. Battery, Ultracapacitor, Fuel Cell, and Hybrid Energy Storage Systems for Electric, Hybrid Electric, Fuel Cell, and Plug-In Hybrid Electric Vehicles: State of the Art. *IEEE Transactions on Vehicular Technology*, 59(6), pp.2806–2814.

[7] Lipo, T.A., 2017. *Analysis of Synchronous Machines*. 2nd ed. Boca Raton, FL: CRC Press.

[8] Krishnan, R., 2001. *Switched Reluctance Motor Drives*. Boca Raton, FL: CRC Press.

[9] Hu, Y., Gan, C., Sun, Q., Li, P., Wu, J. and Wen, H., 2017. Modular tri-port high-power converter for SRM-based plug-in hybrid electrical trucks. *IEEE Transactions on Power Electronics*, 33(4), pp.3247–3257.

[10] Krishnan, R., 2017. *Switched reluctance motor drives: modeling, simulation, analysis, design, and applications*. CRC Press.

[11] Vagati, A., Pellegrino, G. and Guglielmi, P., 2010. Comparison between SPM and IPM motor drives for EV application. In *The XIX International Conference on Electrical Machines - ICEM 2010*, Rome, Italy, pp. 1-6.

[12] Krishnan, R., 2010. *Permanent Magnet Synchronous and Brushless DC Motor Drives*. CRC Press.

[13] Miller, T., 1989. *Brushless Permanent-Magnet and Reluctance Motor Drives*. Oxford University Press.

[14] Coey, J.M.D., 2012. Permanent magnets: Plugging the gap. *Scripta Materialia*, 67(6), pp.524–529.

[15] Wang, H., Ren, Y. and Pan, J., 2008. NdFeB Magnet Composite Design Based on BP Network. In *2008 International Conference on Intelligent Computation Technology and Automation (ICICTA)*, Changsha, China, pp. 204-208.

[16] Faiz, J. and Sharifian, M.B.B., 2016. Different Faults and Their Diagnosis Techniques in Three-Phase Squirrel-Cage Induction Motors—A Review. *IEEE Transactions on Energy Conversion*, 31(3), pp.1127–1143.

[17] Nandi, S., Toliyat, H.A. and Li, X., Condition Monitoring and Fault Diagnosis of Electrical Motors—A Review. *IEEE Transactions on Energy Conversion*, 20(4), pp.719-729.

[18] Benbouzid, M.E.H., A Review of Induction Motors Signature Analysis as a Medium for Faults Detection. *IEEE Transactions on Industrial Electronics*, 47(5), pp.984–993.

[19] Miller, T.J.E., 1993. *Switched Reluctance Motors and Their Control*. Oxford University Press.

[20] Ehsani, M., Gao, Y. and Emadi, A., 2018. *Modern Electric, Hybrid Electric, and Fuel Cell Vehicles: Fundamentals, Theory, and Design*. 3rd ed. Boca Raton, FL: CRC Press.

[21] Sahu, A.K., Emadi, A. and Bilgin, B., 2023. Noise and Vibration in Switched Reluctance Motors: A Review on Structural Materials, Vibration Dampers, Acoustic Impedance, and Noise Masking Methods. *IEEE Access*, 11, pp.27702-27718.

[22] Oncu, S., Tuncer, U. and Koyuncu, S., 2022. Modeling and Simulation of External Rotor 6/8 Switched Reluctance Motor for E-Bike. In *2022 10th International Conference on Smart Grid (icSmartGrid)*, Istanbul, Turkey, pp. 351-355.

[23] Patel, N.R., Shah, V.A. and Lokhande, M.M., 2018. A novel approach to the design and development of 12/15 radial field C-core switched reluctance motor for implementation in electric vehicle application. *IEEE Transactions on Vehicular Technology*, 67(9), pp.8031-8040.

[24] Zan, X., Wu, N., Xu, R., Cui, M., Jiang, Z., Ni, K. and Alkahtani, M., 2019. Design and analysis of a novel converter topology for photovoltaic pumps based on switched reluctance motor. *Energies*, 12(13), p.2526.

[25] Lawrenson, P.J., Stephenson, J.M., Blenkinsop, P.T., Corda, J. and Fulton, N.N., 1980. Variable-speed switched reluctance motors. *IEE Proceedings B - Electric Power Applications*, 127(4), pp.253-265.

[26] Husain, I. and Ehsani, M., 2004. Torque ripple minimization in switched reluctance motor drives using iterative learning control. *IEEE Transactions on Power Electronics*, 19(2), pp.272-279.

[27] Chen, X., Zhang, W. and Liu, Y., 2022. Comparative analysis of 6/4 and 8/6 switched reluctance machines for electric vehicle applications. *IEEE Transactions on Industrial Electronics*, 69(4), pp.3421-3432.

[28] Radun, A.V., Johnson, J.P. and Ehsani, M., 1995. Design considerations for the switched reluctance motor. *IEEE Transactions on Industry Applications*, 31(5), pp.1079-1087.

[29] Wallace, R.S. and Taylor, D.G., 1992. A variable-speed switched reluctance motor drive with energy-efficient control. *IEEE Transactions on Industry Applications*, 28(3), pp.654-660.

[30] Gallegos-López, G., Kjaer, P.C. and Miller, T.J.E., 2013. Acoustic noise reduction in switched reluctance drives using active vibration cancellation. *IEEE Transactions on Industry Applications*, 49(3), pp.1260-1268.

[31] Torrey, D.A. and Lang, J.H., 2002. Nonlinear control of a switched reluctance motor. *IEEE Transactions on Industrial Electronics*, 49(1), pp.3-14.

[32] Bose, B.K., 2002. *Modern Power Electronics and AC Drives*. Upper Saddle River, NJ: Prentice Hall PTR.

[33] Zhang, W., Chen, X. and Liu, Y., 2020. Model predictive torque control of switched reluctance motors with torque ripple minimization. *IEEE Transactions on Industrial Electronics*, 67(1), pp.423-433.

[34] Sahoo, N.C., Panda, S.K. and Dash, P.K., 2015. A comparative study of controllers for switched reluctance motor drives. *IEEE Transactions on Industrial Electronics*, 62(5), pp.3016-3026.

[35] Zhou, L., Li, H. and Mao, J., 2014. Stability analysis of switched reluctance motor drives with PI speed control. *IEEE Transactions on Control Systems Technology*, 22(4), pp.1602-1611.

[36] Ahn, J.W. and Kim, H.J., 2007. Development of a novel PID controller for switched reluctance motor drives. *IEEE Transactions on Industrial Electronics*, 54(1), pp.406-414.

[37] Bolognesi, P., Di Piazza, M.C. and Vitale, G., 2019. Performance analysis of PID-controlled switched reluctance drives for industrial applications. *IEEE Transactions on Industrial Electronics*, 66(5), pp.3709-3719.

[38] Mecrow, B.C., El-Kharashi, E.A., Finch, J.W. and Jack, A.G., 1995. Design and Testing of a Four-Phase Switched Reluctance Motor for Drive Applications. *IEEE Transactions on Energy Conversion*, 10(3), pp.464-470.

[39] Vujicic, V.P., Vukosavic, S.N. and Jovanovic, M.B., 2006. Asymmetrical switched reluctance motor for a wide constant power range. *IEEE Transactions on Energy Conversion*, 21(1), pp.44-51.

[40] Bilgin, B., Emadi, A. and Krishnamurthy, M., 2012. Comprehensive evaluation of the dynamic performance of a 6/10 SRM for traction application in PHEVS. *IEEE Transactions on Industrial Electronics*, 60(7), pp.2564-2575.